Author manuscript of article published in Bioconjugate Chemistry (2021) https://doi.org/10.1021/acs.bioconjchem.1c00251

Photooxidation responsive elastin-like polypeptide conjugates for PDT application

Vusala Ibrahimova,[†] José A. González-Delgado,[‡] Manon Levêque,[†] Tomas Torres,*[‡, ǁ, §] Elisabeth Garanger,*[†] and Sébastien Lecommandoux*[†]

[†] Univ. Bordeaux, CNRS, Bordeaux INP, LCPO, UMR 5629, F-33600, Pessac, France

[‡] Departamento de Química Orgánica, Universidad Autónoma de Madrid, 28049 Madrid, Spain

[ǁ] IMDEA-Nanociencia, Campus de Cantoblanco, 28049 Madrid, Spain

[§] Institute for Advanced Research in Chemical Sciences (IAdChem), Universidad Autónoma de Madrid, 28049 Madrid, Spain

Corresponding authors: lecommandoux@enscbp.fr; garanger@enscbp.fr; tomas.torres@uam.es

ABSTRACT: Stimuli-responsive recombinant elastin-like polypeptides (ELPs) are artificial protein polymers derived from the hydrophobic domain of tropoelastin that have attracted significant interest for drug delivery and tissue engineering applications. In the present study, we have conjugated a photosensitizer (PS) to a hydrophobic methionine-containing ELP scaffold, which upon reaction with singlet oxygen ($^1O_2$) is transformed into a hydrophilic sulfoxide derivative facilitating the disassembly of photosensitizer-delivery particles during the PDT process. A peripherally substituted carboxy-Zn(II)-phthalocyanine derivative (TT1) bearing a carboxyl group directly linked to the Pc-ring, and presenting an absorption maximum around 680 nm, was selected as PS which simultaneously acted as a photooxidation catalyst. A *TT1*-ELP[M_1V_3-*40*] conjugate was prepared from ELP[M_1V_3-*40*] modified with an alkyne group at the *N*-terminal chain end, and from TT1-amide-C3-azide by copper(I)-catalyzed alkyne-azide cycloaddition (CuAAC) reaction. This innovative model photooxidation sensitive PS delivery technology offers promising attributes in terms of temperature-controlled particle formation and oxidation-triggered release, narrow molar mass distribution, reproducibility, scalability, non-immunogenicity, biocompatibility and biodegradability for pharmaceutical applications in an effort to improve the clinical effectiveness of PDT treatments.

KEYWORDS: Elastin-like polypeptide, photodynamic therapy, carboxy Zn(II)-phthalocyanine, photooxidation, stimuli-responsive self-assembly, bioconjugate

INTRODUCTION

Photodynamic therapy (PDT) is an attractive non-invasive cancer treatment alternative with higher selectivity and lower side effects as compared to conventional methods like surgery, chemotherapy, and radiotherapy.[1,2] The main components of PDT, namely a photosensitizer (PS), light, and oxygen, are non-toxic individually, while locally generating highly toxic reactive oxygen species (ROS) when used in combination *via* energy or electron transfer from the excited triplet state of the PS to nearby molecular oxygen.[3] This can imply the selective activation of non-toxic photosensitizers accumulated at tumor sites with NIR light (600-800 nm).[4,5] During photo-irradiation, generated ROS cause multiple oxidative damages to the surrounding microenvironment impairing malignant cells' metabolic function leading to apoptosis and/or necrosis.[6,7] Small scale inflammations, occurring after PDT anti-cancer treatment, have also been shown to activate the natural immune system against malignant cells, resulting in the complete destruction of the tumor and limiting the risk of tumor recovery.[8] Together with low dark toxicity, the success of PDT mainly relies on the photophysical properties of the selected PS (extinction coefficient (ε), singlet oxygen ($^1O_2$) generation quantum yield (Φ_Δ), *etc*.) and its effective accumulation at the tumor site.[1,9-11] Phthalocyanine (Pc) derivatives, considered as second generation PS, are synthetic formal derivatives of porphyrins, with superior photophysical properties and high chemical versatility.[10] Several Pc-based photosensitisers (Photosens, Photocyanine, Pc 4, IRDye®700DX) have been approved for clinical use or are in advanced stages of clinical trials.[12,13] Further development of these phototherapeutic agents, both at the molecular level and as nanometer-sized formulations, is currently of strong interest. Pc derivatives are composed of four pyrrole subunits each one fused with an additional benzo ring and linked *via* nitrogen atoms. Extended conjugation and lone electron pairs on nitrogen atoms significantly increase electron density of the Pc backbone causing a red-shifting of the absorption wavelength and increasing the absorption coefficient, which are two essential parameters for effective PDT performance in complex biological media.[11] Pc metal ion chelates (Zn^{2+}, Al^{3+}, Mg^{2+}, Ru^{2+}, *etc*.) generally show efficient triplet state

population, and consequently an increased $^1O_2$ generation yield.[12,14,15] Due to the intrinsic hydrophobicity of Pcs, hydrophilic derivatives have been developed. Nevertheless and besides synthetic challenges, the uncontrolled aggregation tendency of Pc backbones combined with their low molar mass leads to uncontrolled biodistribution of this class of PS in the body. In this context, several studies have shown that macromolecular conjugates or nanocarriers of PSs improve their biodistribution, bioavailability and therapeutic outcome by increasing their solubility and plasma half-life, and avoiding fast renal clearance.[16-18] A wide variety of synthetic and natural biocompatible polymers have been developed for nanomedicine applications, especially for the design of complex drug delivery vehicles.[17] Among these, recombinant elastin-like polypeptides (ELPs) have attracted significant interest for drug delivery and tissue engineering applications due to their biocompatibility, biodegradability, low immunogenicity and stimuli-responsive properties.[19,20] ELPs are artificial protein polymers derived from the hydrophobic domain of tropoelastin, the soluble precursor of elastin, and consists in repetitive sequences of [-Val-Pro-Gly-Xaa-Gly-] pentapeptides.[21] Their inverse phase transition behavior provides a unique opportunity to engineer sophisticated stimuli-responsive delivery systems.[20,22-24] Indeed, ELPs present lower critical solution temperature (LCST) phase behavior: below their critical aggregation temperature at a given concentration (cloud point, noted as T_{CP}), ELP chains are soluble and mostly intrinsically disordered, while hydrophobically collapsing above the T_{CP}. Our group has in particular developed chemoselectively modifiable recombinant ELP scaffolds for easy tuning of their thermal responsiveness by chemical modification.[22,25-27] In particular, we have engineered methionine-containing ELP scaffolds that can be chemoselectively modified at the side chain of each methionine residue to tune their physico-chemical properties or to introduce specific functionalities.[25,26,28-30] Due to its sensitivity to oxidation, the thioether group of methionine can also be readily oxidized into sulfoxide, turning a hydrophobic methionine-containing ELP with low T_{CP} into a hydrophilic sulfoxide derivative with high T_{CP}.[22] In the present work, we show that this characteristic property can be used to

develop smart temperature and singlet oxygen responsive ELP-PS conjugates as illustrated in Figure 1.

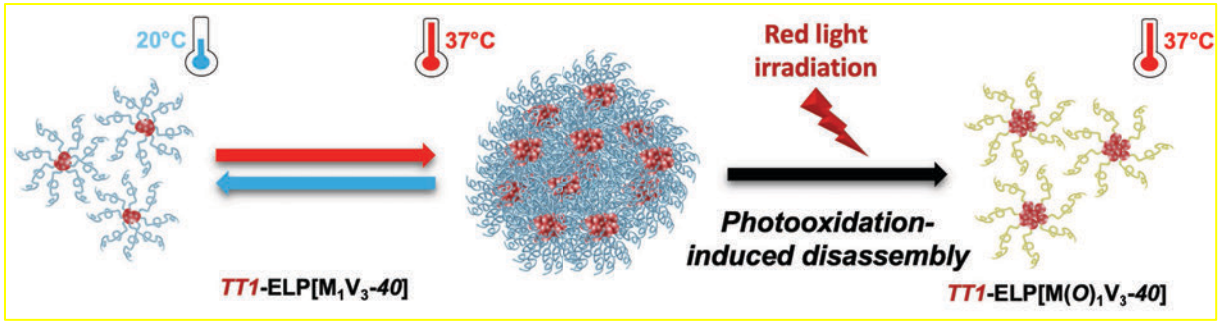

Figure 1. Proposed mechanism of assembly of *TT1*-ELP[M_1V_3-*40*] conjugates into micellar coacervates at 37°C and disassembly into individual micelles upon photoirradiation.

Towards this goal, an ELP containing 40 (VPGXG) pentapeptide repeats with X=M/V (1:3) (denoted ELP[M_1V_3-*40*]) was conjugated at the *N*-terminal chain end with a Zn(II)-phthalocyanine PS (noted TT1). Upon specific photo-irradiation of the PS, ELP[M_1V_3-*40*] was found to be oxidized into its sulfoxide derivative ELP[M(*O*)$_1V_3$-*40*] turning the hydrophobic *TT1*-ELP[M_1V_3-*40*] conjugate, which self-assembled into large micellar coacervates at physiological body temperature, into an amphiphilic *TT1*-ELP[M(*O*)$_1V_3$-*40*] conjugate self-assembled into small micelles, that shall diffuse more easily in dense tumors allowing for a second photo-irradiation and even more efficient PDT.

RESULTS AND DISCUSSION

The ELP used in the present work, namely ELP[M_1V_3-*40*] with the exact protein sequence MW[(VPGVG)(VPGMG)$(VPGVG)_2]_{10}$ was produced recombinantly in *Escherichia coli* (*E. coli*) bacteria following previously reported procedures.[22,25] A peripherally substituted carboxy-Zn(II)-phthalocyanine derivative (TT1) was selected as photosensitizer due to its outstanding photo-physical properties.[31-33] It has a carboxyl group directly linked to the Pc-ring and exhibits an excellent absorption coefficient around 680 nm ($\varepsilon \sim 10^5$ $M^{-1}.cm^{-1}$), whereas its UV-Vis spectrum offers a broad therapeutic optical window. Such a design of photosensitizers in the near-infrared (NIR)

window (650–950 nm), also referred as the "therapeutic window", is specifically relevant for biomedical applications as the absorption by other chromophores and/or by the tissues is minimized, allowing for a most effective laser therapy. The singlet oxygen quantum yield of TT1 measured in DMSO mounts up to $\Phi_\Delta = 0.72$. The presence of *tert*-butyl groups not only minimizes the formation of molecular aggregates,[31] but also increases the solubility of TT1 in organic solvents. TT1 is actually constituted of a mixture of eight regioisomers, in equal proportions. TT1 was synthesized according to a previously described procedure.[31] The compound was then reacted with 3-azidopropylamine, COMU® ({[(Z)-(1-Cyano-2-ethoxy-2-oxoethylidene)amino]oxy}-*N*,*N*-dimethyl(morpholin-4-yl)methaniminium hexafluorophosphate), and diisopropylethylamine in DMF to yield TT1-amide-C3-azide in 75% yield. (**Scheme S1**, **Figure S1-3**)

The ***TT1***-ELP[M_1V_3-***40***] conjugate was then prepared from ELP[M_1V_3-***40***] modified with an alkyne group at the *N*-terminal chain end following a protocol established by our group,[27] and from TT1-amide-C3-azide by copper(I)-catalyzed alkyne-azide cycloaddition (CuAAC) reaction in DMSO. (**Scheme 1**) The reaction mixture was extensively degassed *via* freeze-thaw cycles under vacuum to prevent oxidation of methionine residues. Excess copper was removed by treatment of the reaction mixture with Cuprisorb® beads followed by filtration, and the reaction product was precipitated with diethyl ether. The precipitate was dissolved in ultrapure water and further purified by inverse transition cycling (ITC)[34] yielding the pure ***TT1***-ELP[M_1V_3-***40***] conjugate, as assessed by different analytical techniques, in 80% overall yield. Quantitative modification at the ELP chain end and complete removal of excess TT1 used for the reaction were confirmed by MALDI MS, SDS-PAGE and SEC analyses. (**Figure 2A-C**) MALDI MS analysis of ***TT1***-ELP[M_1V_3-***40***] showed a single peak at 18,033.5 in perfect agreement with the theoretical molar mass. (**Figure 2A** and **Table 1**)

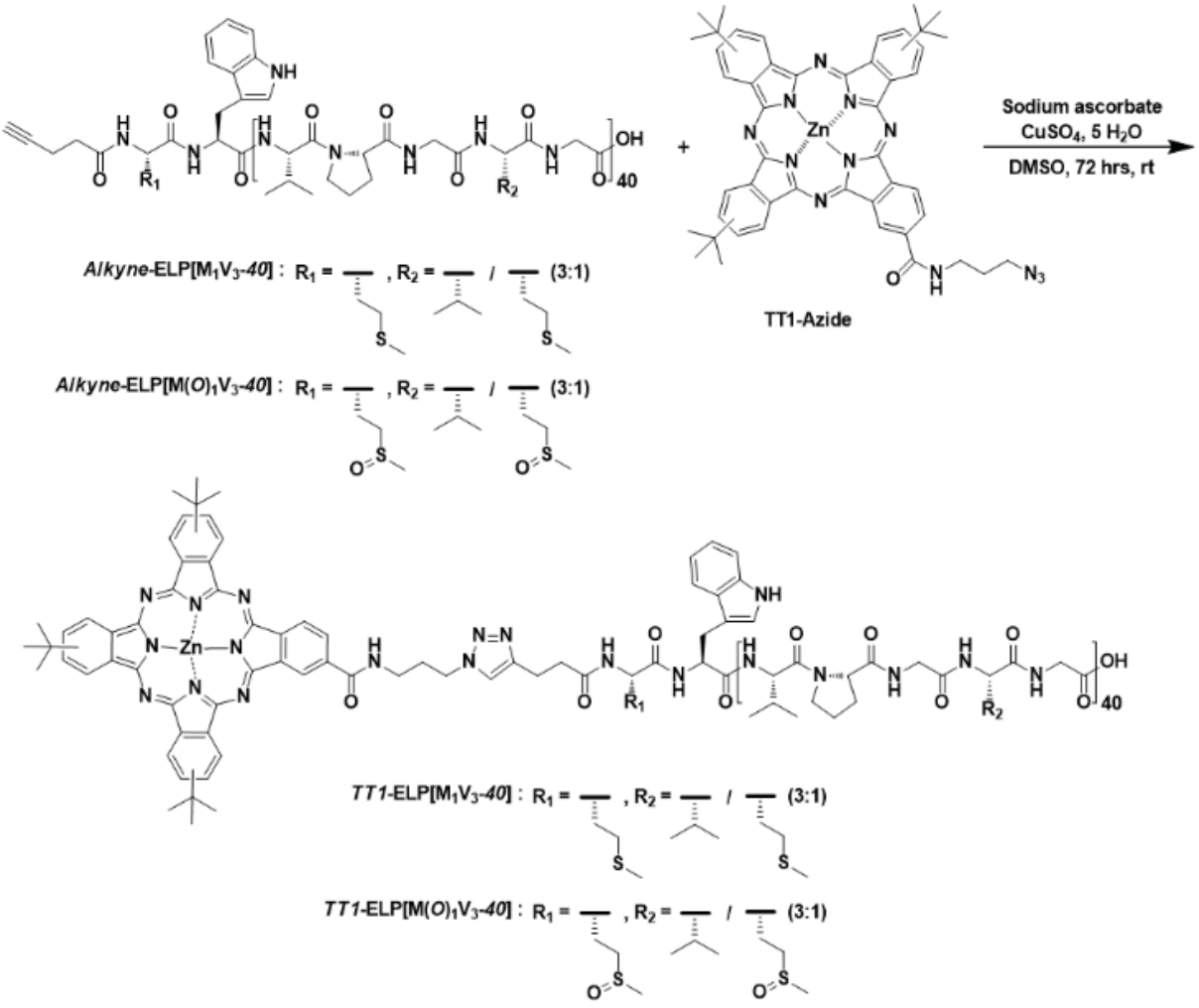

Scheme 1. Synthetic scheme to access *TT1*-ELP[M_1V_3-*40*] and the reference compound *TT1*-ELP[$M(O)_1V_3$-*40*].

SDS-PAGE analysis showed the successful removal of excess TT1 used for the reaction. (**Figure 2B** and **Figure S4**) The SEC chromatogram of *TT1*-ELP[M_1V_3-*40*] (RI detection) revealed a monomodal peak distribution. (**Figure 2C**) The presence of a small shoulder at shorter retention times is attributed to aggregates of *TT1*-ELP[M_1V_3-*40*] due to π-π stacking of the TT1 planar backbone. Absorption at 607 nm also indicated the successful attachment of TT1 to the ELP chain end. (**Figure 2C**)

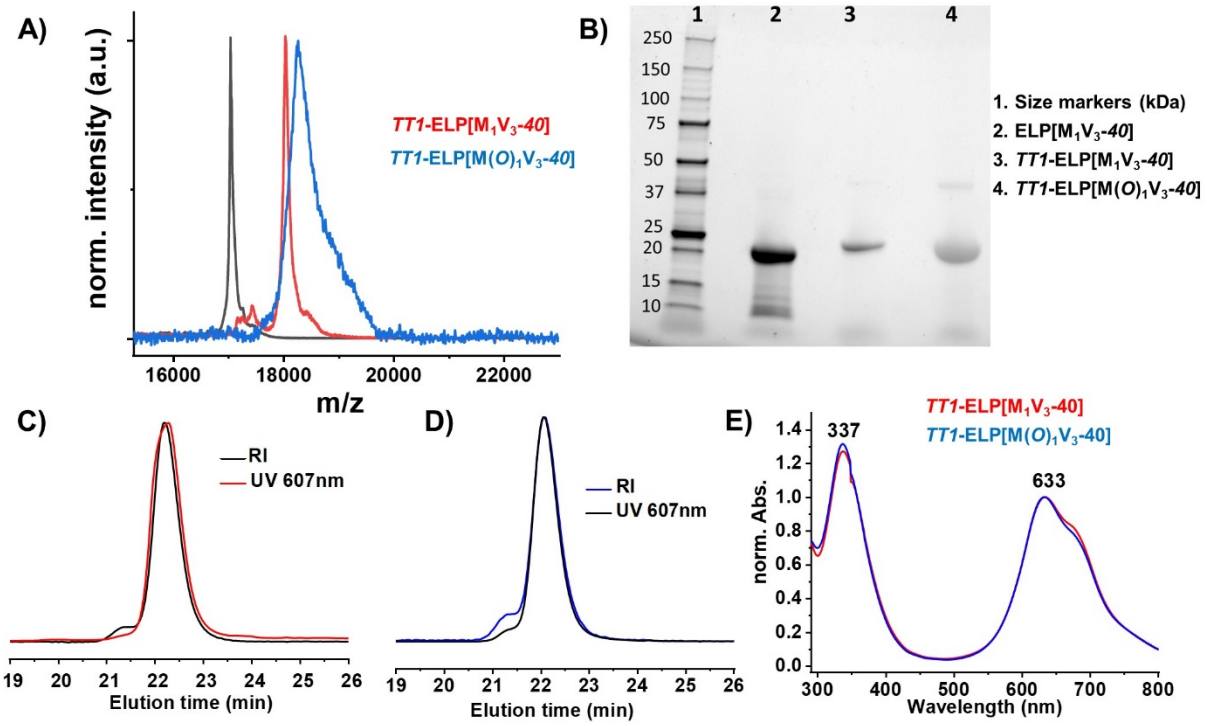

Figure 2. Characterization of *TT1*-ELP[M_1V_3-*40*] and *TT1*-ELP[$M(O)_1V_3$-*40*] conjugates. (A) Superimposed MALDI mass spectra of *TT1*-ELP[M_1V_3-*40*] and *TT1*-ELP[$M(O)_1V_3$-*40*]. The spectrum of ELP[M_1V_3-*40*] is provided for comparison (black trace). (B) SDS-PAGE analysis. (C) Size exclusion chromatogram of *TT1*-ELP[M_1V_3-*40*] in DMSO (red trace: RI detection; black trace: UV detection at 607 nm). (D) Size exclusion chromatogram of *TT1*-ELP[$M(O)_1V_3$-*40*] in DMSO (blue trace: RI detection; black trace: UV detection at 607 nm). E) Overlapped absorption spectra of *TT1*-ELP[M_1V_3-*40*] (red trace) and *TT1*-ELP[$M(O)_1V_3$-*40*] (blue trace) in PBS buffer at 25 °C.

^{1}H NMR spectroscopy was performed at 5 °C to insure full solubility of *TT1*-ELP[M_1V_3-*40*]. A slight oxidation of methionine residues (8%, *i.e.* less than one methionine over a total of 11) was observed which may have been caused by short term light exposure during sample preparation or during analysis. (**Figure S5**)

Methionine residue oxidation in proteins is a natural mechanism used in mammalian cells to deactivate the small amounts of ROS generated and accumulated in the body.[35,36] These so called antioxidant proteins can be recovered *via* MSR enzymes (methionine sulfoxide reductases) by reducing the sulfoxide to repair the original methionine.[36] Because in this study the designed ELP[M_1V_3-*40*] contains periodically spaced

methionine residues prone to oxidation, and therefore highly sensitive to reactive oxygen species, we hypothesized that photo-irradiation of *TT1*-ELP[M_1V_3-*40*] would oxidize the methionine thioether groups (11 total in the sequence of ELP[M_1V_3-*40*]), increase the T_{CP} of the conjugate due to increased polarity,[22] and possibly trigger the disassembly of micellar coacervates formed at physiological body temperature.

To verify this hypothesis, we have synthesized in parallel the reference compound noted *TT1*-[M(*O*)$_1$$V_3$-*40*] in which all methionine residues are oxidized into sulfoxide form. The latter was obtained from the sulfoxide derivative ELP[M(*O*)$_1$$V_3$-*40*] functionalized with an alkyne group at the *N*-terminal chain end, and from TT1-amide-C3-azide by CuAAC reaction in DMSO, and purified following similar procedures to those used for *TT1*-ELP[M_1V_3-*40*]. (**Scheme 1**) ELP[M(*O*)$_1$$V_3$-*40*] was obtained by oxidation of the pristine ELP[M_1V_3-*40*] with hydrogen peroxide (H_2O_2) following a protocol established by our group.[22] (**Figures S6-7**) The quantitative oxidation of ELP[M_1V_3-*40*] was monitored by ^{1}H NMR (**Figure S6**) as well as the complete functionalization of the *N*-terminal chain end. (**Scheme S2** and **Figure S8**) TT1-amide-C3-azide conjugation to *Alkyne*-ELP[M(*O*)$_1$$V_3$-*40*] was confirmed by MALDI MS, SDS-PAGE, SEC, UV-Vis spectroscopy, and ^{1}H NMR analyses. (**Figure 2A, B, D, E** and **Figure S9**) MALDI MS analysis showed a shift of 1,174 Da between the monocharged species, $[M+H]^+$, of ELP[M_1V_3-*40*] and *TT1*-ELP[M(*O*)$_1$$V_3$-*40*] in good agreement with the theoretical value (1,177 Da). (**Figure 2A** and **Table 1**) The SEC chromatogram of *TT1*-ELP[M(*O*)$_1$$V_3$-*40*] (RI detection) showed a narrow monomodal peak distribution which overlapped with the UV detector signal at 607 nm indicating successful conjugation of TT1. (**Figure 2D**)

Table 1. Characteristics of ELP derivatives synthesized.

Compound notation	MW^{theo} (Da)	$[M+H]^+$ MALDI MS (Da)	λ_{max} (nm) in PBS	SEC in DMSO	
				Mn (Da)	Đ
ELP[M_1V_3-*40*]	17,035.4	17,039.6		17,610	1.087
TT1-ELP[M_1V_3-*40*]	18,032.9	18,033.5	337 & 633	20,120	1.129
ELP[M(*O*)$_1$$V_3$-*40*]	17,211.4	n.d.		19,841	1.177

TT1-ELP[M(*O*)$_1$V$_3$-*40*]	18,212.7	18,213.79	337 & 633	20,710	1.239

n.d. not determined

The thermo-responsive character of ELP[M_1V_3-*40*], before and after TT1 conjugation, was measured by turbidity assays in phosphate buffer (PBS, pH 7.4) following the absorbance at 600 and 500 nm, respectively, over a temperature range from 10 to 65 °C. Measurements were performed at three concentrations (10, 20 and 30 μM) at which *TT1*-ELP[M_1V_3-*40*] is fully soluble at 10 °C. At these concentrations, the transition temperature (T_{CP}) of the pristine ELP[M_1V_3-*40*] was in the range of 35-38 °C, close to physiological body temperature which is relevant with literature results for short chain length ELPs,[37] and in full concordance with our previous studies.[22] (**Table 2**) After conjugation of TT1, the T_{CP} was found to drop by approximately 10 °C, the T_{CP} of *TT1*-ELP[M_1V_3-*40*] ranging from 29 °C at 10 μM to 27 °C at 30 μM. (**Table 2, Figure S10A**)

Table 2. Summary of the transition temperature (T_{CP}) of the different ELP conjugates.

Compound name	T_{CP} in PBS (°C)[a]			T_{CP} in PBS (°C)[b]
	10 μM	20 μM	30 μM	30 μM
ELP[M_1V_3-*40*]	38	36	35	
TT1-ELP[M_1V_3-*40*]	29	28	27	27
TT1-ELP[M(*O*)$_1$V$_3$-*40*]	46	46	45	44
TT1-ELP[M_1V_3-*40*]^{PhOx}	45	45	44	

PhOx: photooxidized

[a] Determined by UV-Vis spectroscopy. [b] Determined by dynamic light scattering.

[a,b] Measured upon a temperature ramp. The T_{CP} corresponds to the onset temperature where the signal (absorbance or derived count rate, respectively) starts increasing.

This was expected due to the strong hydrophobic character of TT1. The insertion of a hydrophobic molecular domain increases intra- and intermolecular hydrophobic interactions in the ELP backbones.[38] In addition, dynamic light scattering evidenced the formation of very small micelles with a hydrodynamic diameter D_H ~ 31±2 nm below T_{CP} of *TT1*-ELP[M_1V_3-*40*] as a consequence of TT1 intermolecular hydrophobic interactions (**Figure S11**). This self-assembly mechanism, that locally increases the ELP concentration, also explains the lower T_{CP}. Above the T_{CP} of *TT1*-ELP[M_1V_3-*40*] around

27 °C, larger micellar coacervates of 2.7 µm could be observed, suggesting that *TT1*-ELP[M_1V_3-*40*] would be aggregated when used *in vivo*. In clinical application, these smart particles could be disassembled upon local cryothermia[39] at the tumor to let the small micelles of *TT1*-ELP[M_1V_3-*40*] diffuse deeper into the tumor mass before applying the PDT treatment.

Interestingly, the disassembly of *TT1*-ELP[M_1V_3-*40*] coacervates could also be triggered by oxidation of methionine residues by $^1O_2$ generated upon TT1 activation by NIR light. Indeed, the thermo-responsive behavior of the chemically oxidized conjugate *TT1*-ELP[$M(O)_1V_3$-*40*] measured in similar conditions to those used for *TT1*-ELP[M_1V_3-*40*] (PBS, pH 7.4) showed a huge jump (~17 °C) in T_{CP} as compared to the non-oxidized conjugate. (**Table 2, Figure 4A, B** and **Figure S10C**) With a T_{CP} of ca. 45 °C, well above body temperature, the oxidized conjugate *TT1*-ELP[$M(O)_1V_3$-*40*] coacervates shall therefore be destabilized at 37 °C.

As a proof of concept, a solution of *TT1*-ELP[M_1V_3-*40*] in D_2O was therefore subjected to irradiation with a red-light emitting diode (LED, 630-640 nm) and ^{1}H NMR spectroscopy used to follow the selective oxidation of methionine residues. The formation of sulfoxide during the red emitting LED irradiation over 5, 10, 15, 20 and 30 minutes was monitored by the shift of the resonance peak at 2.1 ppm attributed to the protons of the methyl group adjacent to the sulfur in the thioether form (-SCH_3) to 2.6 ppm in the sulfoxide form (-S(O)CH_3). (**Figure 3A**) Approximately 50% oxidation was observed in 5 min, while 30 min irradiation caused complete oxidation of the 11 methionine residues of the ELP. We also noticed an increased spectral resolution of ^{1}H NMR analyses performed at room temperature during the photooxidation process as a result of higher solubility of the conjugate formed noted *TT1*-ELP[M_1V_3-*40*]^{PhOx}. The overlapped SEC chromatograms of *TT1*-ELP[M_1V_3-*40*]^{PhOx} showed narrow monomodal peak distribution confirming the selectivity of the oxidation process without any traces

of crosslinking or degradation in the backbone. (**Figure 3B**) Increased dimer population displayed in SEC and also observed in SDS-PAGE gel (**Figure 3C**), is probably due to the strong hydrophobic interactions between TT1 chain ends.

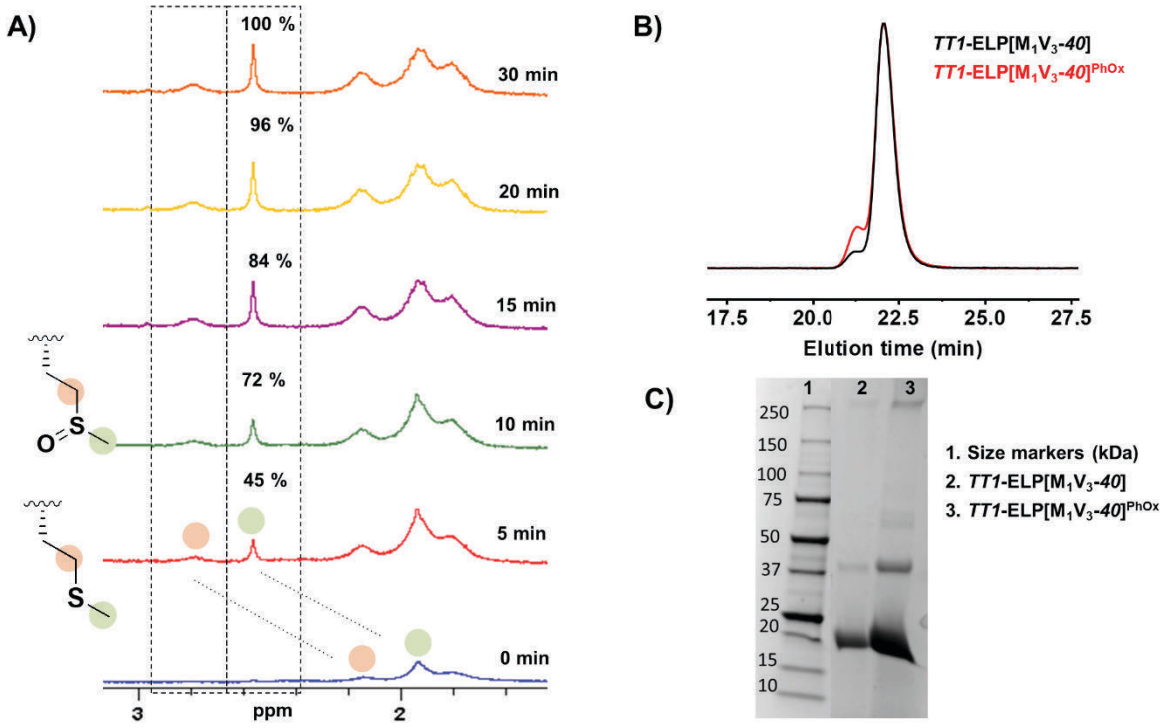

Figure 3. (A) Stacked ^{1}H NMR spectra of *TT1*-ELP[M_1V_3-*40*] after photoirradiation during 5, 10, 15, 20, and 30 minutes (D_2O, room temperature, 200 MHz). (B) SEC chromatograms in DMSO of *TT1*-ELP[M_1V_3-*40*] before (black curve, RI detection) and after photoirradiation (red curve, RI detection). (C) SDS-PAGE analysis (coomassie blue stain).

The thermo-responsive character of the photo-oxidized conjugate, *TT1*-ELP[M_1V_3-*40*]^{PhOx}, was also measured by turbidimetry and compared to the one of the starting *TT1*-ELP[M_1V_3-*40*] conjugate and of the reference compound *TT1*-ELP[M(*O*)$_1V_3$-*40*]. The T_{CP} at 30 µM in PBS was shifted from 27 °C for *TT1*-ELP[M_1V_3-*40*] to 44 °C (**Figure 4A, B** and **Figure S10B**) in perfect agreement with the value obtained for the chemically synthesized sulfoxide version *TT1*-ELP[M(*O*)$_1V_3$-*40*]. (**Table 2** and **Figure S10C**) One would expect a drastic change in physicochemical properties of the ELP backbone resulting from the sulfoxide formation, with a shift of the phase transition temperature of the conjugate and a destabilization and disassembly of the coacervates observed at body temperature.

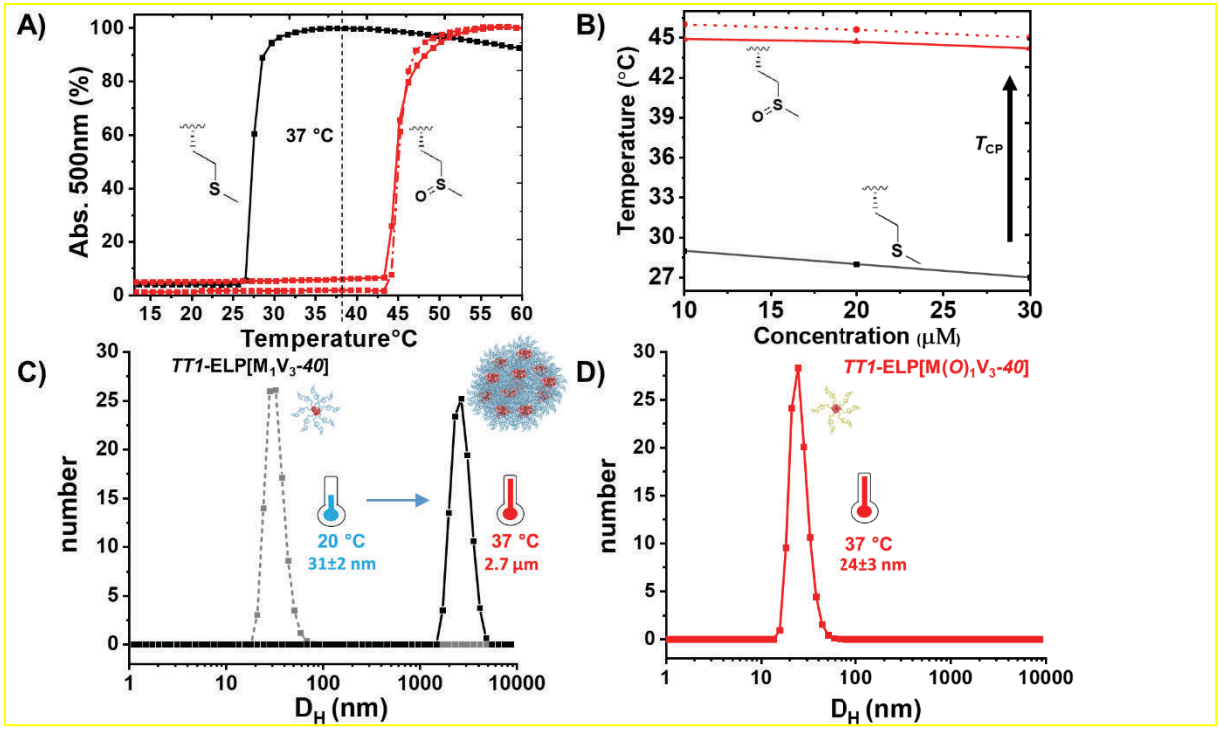

Figure 4. A) Normalized relative absorbance at 500 nm of 30 μM solution of *TT1*-ELP[M_1V_3-*40*] (black trace), *TT1*-ELP[M_1V_3-*40*]^{PhOx} (red trace) and *TT1*-ELPM(O)$_1$$V_3$-*40*] (red dots) conjugates in PBS as a function of temperature. B) Transition temperature (T_{CP}) versus molar concentration of *TT1*-ELP[M_1V_3-*40*] (black), *TT1*-ELP[M_1V_3-*40*]^{PhOx} (red) and *TT1*-ELP[M(O)$_1$$V_3$-*40*] (red dots). C) Size distribution (in number) of *TT1*-ELP[M_1V_3-*40*] at 20 °C and 37 °C (30 μM concentration in PBS). D) Size distribution (in number) of *TT1*-ELPM(O)$_1$$V_3$-*40*] at 37 °C (30 μM concentration in PBS).

In order to mimic the self-assembly and photooxidation-triggered disassembly profile of *TT1*-ELP[M_1V_3-*40*], dynamic light scattering (DLS) measurements were performed in physiological conditions (PBS pH 7.4 at 37 °C) (**Figure 4C).** Due to the tendency of TT1 to aggregate,[31,33] upon direct dissolution of *TT1*-ELP[M_1V_3-*40*] in PBS at ambient temperature (20 °C), small micelles with a hydrodynamic diameter D_H ~ 31±2 nm were observed. (**Figure 4C**) Temperature-controlled high-speed AFM imaging also confirmed the presence of the micelles even at 15 °C. (**Figure S12A**) Nevertheless, the strong absorption of the laser light used in the liquid AFM equipment by self-assembled particles above 37 °C prevented from obtaining a clear topological image. (**Figure**

S12B). Increase of the solution temperature to 37 °C resulted in the formation of large coacervates (*ca.* 2.7 μm hydrodynamic diameter) in PBS (pH 7.4), while dropping the temperature back to 20 °C leads to the disassembly of these aggregates back to small micelles (D_H ~ 31±2 nm). (**Figure 4C**) In contrast, DLS analysis of *TT1*-ELP[M(O)$_1$V$_3$-*40*] at 37 °C in PBS (pH 7.4) evidenced only the presence of small micelles (D_H ~ 24±3 nm) with no larger coacervates. (**Figure 4D**)

We believe this experimental demonstration of the multi-responsive behavior of this PS delivery system to be potentially very interesting in terms of clinical applications. Indeed, one could expect that self-assembled *TT1*-ELP[M$_1$V$_3$-*40*] conjugates accumulated at the tumor site would disassemble upon local photoirradiation (PDT^1) due to methionine residues oxidation and increase of T_{CP}. Soluble photo-oxidized micellar conjugates would consequently diffuse deeper into the tumor tissue and improve the efficacy of a second photoirradiation (PDT^2) as illustrated in **Figure 1.** The reactivation of photosensitizers (PDT^2) may then cause considerable damage to the tumor mass and maximize therapeutic benefit.

Furthermore, therapeutic efficacy of PSs strongly depends on their optical and photo-physical properties. Optical characterization of TT1-ELP conjugates at ambient temperature showed no difference in absorption maxima at PBS buffer (pH 7.4, λ_{abs}=337 and 633 nm). (**Figures 2E**) Owing to the conjugation to the polypeptide, aqueous environment with higher ionic strength and stacking of TT1 chain ends, the absorption peaks of the conjugates get broader and blue-shifted from 673 nm (TT1 in THF) to 633 nm (conjugate in PBS). The TT1 dimer/multimer formation in the unfavorable solvent (PBS buffer) also quenches the fluorescence property, nevertheless this has no remarkable effect on the singlet oxygen generation property. The comparison of the absorption spectrum of *TT1*-ELP[M$_1$V$_3$-*40*]^{PhOx} with the control compound *TT1*-ELP[M(O)$_1$V$_3$-*40*] in water revealed slight decrease in absorption band at 630 nm despite the long light exposure (30 min LED, 650 nm) where the absorption at 339 nm remains

unchanged, indicating the potential photostability of TT1 during long lasting phototherapies. (**Figure S13**)

Conclusions

Nature-inspired genetically engineered recombinant ELPs are remarkable smart polypeptides for biomedical applications owing to their controlled molecular weight, exquisite design, thermal responsiveness, biocompatibility and non-immunogenicity.[40] In addition, the cost effective production in large scale with precise control on molecular composition makes them excellent drug delivery matrix polymers that can deliver and release a targeted drug (PS) in response to external stimuli.[41,42] Here we experimentally demonstrated a new approach for the delivery of a photosensitizing molecule, namely a peripherally substituted carboxy-Zn(II)-phthalocyanine (TT1), to be used in PDT cancer treatment by using Met's ROS scavenging property to trigger the disassociation of self-assembled micellar coacervates due to the emerging oxidized chain. To this end, we have prepared a *TT1*-ELP[M_1V_3-*40*] conjugate from recombinant ELP[M_1V_3-*40*] modified with an alkyne group at the *N*-terminal chain end, and from TT1 functionalized with an azido group. Unlike previously reported drug-ELP conjugates,[19] such conjugates do not require additional treatment such as local hyperthermia to trigger *in vivo* dis-assembly. On the contrary, local disassembly can be promoted by a first PDT treatment that would allow micellar conjugates to diffuse deeper into the tumor tissue enabling a more efficient second PDT. We believe this strategy opens an interesting possibility to construct multi-responsive bioinspired delivery systems with externally controlled hydrophobic association and dissociation properties. Moreover, besides remarkable responsive properties,

this model delivery system offers a quantitative control on PS concentration and prevents its uncontrolled accumulation and leakage before reaching the targeted site.

MATERIALS AND METHODS

Materials

The following reagents have been used as they were received: sodium chloride (NaCl, VWR, 100%), ammonium acetate ($C_2H_3O_2NH_4$, Sigma-Aldrich, BioXtra 98%), acetic acid glacial (CH_3CO_2H, Chem-Labs Limited), *N*, *N*-diisopropylethylamine (DIPEA, Sigma-Aldrich, 99%), copper (II) sulfate pentahydrate (Cu_2SO_4 $5H_2O$, Acros Organics, 98%), (+)-Sodium *L*-ascorbate ($C_6H_7NaO_6$, Sigma-Aldrich, 98%), 9(10),16(17),23(24)-Tri-tert-butyl-2-carboxy-5,28:14,19-diimino-7,12:21,26-dinitrilotetrabenzo[c,h,m,r][1,6,11,16]tetraazacycloeicosinato-(2)-N29,N30,N31,N32 zinc (II) (mixture of regioisomers) (TT1), 3-azidopropylamine ($C_3H_8N_4$, TCI Europe, >95%), COMU® ($C_{12}H_{19}F_6N_4O_4P$, Sigma-Aldrich, 97%), Cuprisorb® (Seachem). The following solvents have been used without further purification: ethanol (EtOH, VWR chemicals, analytical grade, 100%), dichloromethane (DCM, Sigma-Aldrich, analytical grade, 99.9%), *N*, *N*- dimethylformamide (DMF, Fluka, 99.8%), acetonitrile (ACN, VWR chemicals, HPLC grade, 99.9%), diethyl ether (Et_2O, VWR chemicals, 97%), dimethyl sulfoxide (DMSO, Sigma-Aldrich, 99,9%), 1,4-dioxane (Carlo Erba, HPLC - Stabilized with BHT), n-hexane (Carlo Erba, for analysis, 99%).

Experimental procedures

Synthesis of TT1-amide-C3-azide

COMU (16.8 mg, 0.039 mmol) was added to a mixture of TT1 (20 mg, 0.025 mmol), freshly distilled DIPEA (5.3 µL) in dry DMF (0.5 mL) at room temperature under Ar atmosphere. Then, 3-azidopropylamine (4.0 mg, 0.04 mmol) was added dropwise. The reaction mixture was

stirred for 24 h. The mixture was diluted with DCM (2 mL) and extracted with 1N HCl (2 × 5 mL), 1N $NaHCO_3$ (2 × 5 mL) and saturated NaCl (2 × 5 mL). DCM was then dried with $MgSO_4$, the solvent was removed, and the crude was directly purified by flash column chromatography on silica gel (dioxane/n-hexane = 50:50) to give 16.4 mg of 1 (75%) as a dark blue solid. ^{1}H-NMR (300 MHz, DMSO-*d6*): δ 9.91 (m, 1H), 9,55-9,30 (m, 8H), 8,71 (m,1H), 8,37 (m, 3H),3,63 (m, 2H), 2.07-2.02 (m, 2H), 1.78 (s, 27H), 1.24 (m, 2H) ppm. HR-MS (MALDI-TOF, DCTB): Calc. for $C_{48}H_{46}N_{12}OZn$: $[M]^+$: m/z: theoretical 870.3209, experimental 870.3204. UV/Vis: (THF): λ_{max} (nm) (ε) = 673 (4.70); 607 (4.68), 348 (4.08).

General procedures for TT1-ELP conjugates syntheses

Alkyne-ELP (1 equiv.) and TT1 (Zn(II)-phthalocyanine, 2 equiv.) were dissolved in dry DMSO (10 mg mL^{-1}) and $CuSO_4$ 5H2O (1 equiv.) and sodium ascorbate (2 equiv.) were added and the solution was degassed by freeze-pump-thaw cycles. The solution left under stirring for 72 h at room temperature under N_2 atmosphere. Excess copper was removed by Cuprisorb beads and subsequent filtration. The reaction solution was dialyzed (MWCO 3.5 kDa) against ultrapure water for 48h and lyophilized. The final product was purified by inverse transition cycling (ITC) and lyophilized.

General procedures of ITC purification for TT1-ELP conjugates

The blue product was dissolved in 1M NaCl solution (5 mL) and placed on a heating bath (40 °C). Fluctuated conjugates were centrifuged during 10 min at 38 °C (3800 RPM speed). The supernatant was discarded and the dark blue pellet was dissolved in cold water (3 mL). The solution was centrifuged for 30 min at 4 °C (3800 RPM speed) and the pellet was discarded. A few drops of 1 M NaCl solution was added into the supernatant and placed into the heating bath. Aggregated conjugates were centrifuged for 10 min at 38 °C (3800 RPM speed). Finally the supernatant was discarded and the pellet was dissolved in cold ultrapure water and dialyzed

against ultrapure water in a dialysis bag (cut-off MWCO 3.5 kDa) for 24h to remove the excess salt. The solution was lyophilized to obtain pure blue conjugates.

Analysis of *TT1*-ELP[M_1V_3-*40*]

Yield of pure conjugate is 16 mg, 80%.

^{1}H NMR (400 MHz, D_2O, 5 °C): δ 4.38 (br m, 11H αCH Me), 4.28-4.25 (m, 80H αC*H* Val, Pro), 4.00-3.99 (d, 30H αC*H* Val_{xaa}), 3.80-3.77 (br m, 200H αCH_2 Gly, δCH_2 Pro), 3.54 (br , 40H δCH_2 Pro), 2.47-2.35 (br m, 22H γCH_2 Met), 2.16 (br m, 40H βCH_2 Pro), 1.93-1.80 (br m, 240H βCH_2 Met, βCH_2 Pro, γCH_2 Pro, βCH_2 Val, εCH_3 Met), 0.83-0.70 (m, 420 H, γCH_3 Val).

SEC (DMSO, LiBr 1 g L^{-1}, standard: Dextran) Mn = 20120 Da, Mw/Mn = 1.129.

MALDI MS: theoretical MW = 18032.96 Da, experimental $[M+H]^+$ = 18033.521 Da

UV absorption in water λ_{max} = 337, 633 nm, no fluorescence.

Analysis of *TT1*-ELP[M(*O*)$_1$$V_3$-*40*]

Yield of pure conjugate is 13 mg, 58%.

^{1}H NMR (400 MHz, D_2O, 5 °C): δ 4.38 (br, 11H αC*H* Me), 4.25-4.26 (br , 80H αC*H* Val, Pro), 3.98 (br, 30H αC*H* Val_{xaa}), 3.79 (br, 200H αCH_2 Gly, δCH_2 Pro), 3.54 (br, 40H δCH_2 Pro), 2.80 (br , 22H γCH_2 Met), 2.56 (s,33H εCH_3 Met) 2.15 (br, 40H βCH_2 Pro), 1.92-1.70 (br m, 207H βCH_2 Met, βCH_2 Pro, γCH_2 Pro, βCH_2 Val), 0.77 (br, 420 H, γCH_3 Val)

SEC (DMSO, LiBr 1g L^{-1}, standard: Dextran) Mn = 20710 Da, Mw/Mn = 1.239.

MALDI MS: theoretical MW = 18212.766 Da, experimental $[M+H]^+$ = 18213.795 Da

UV absorption in water λ_{max} = 337, 633 nm, no fluorescence.

Nuclear Magnetic Resonance (NMR): ^{1}H NMR spectra were recorded with a Bruker AVANCE III HD (Liquid-state 400 MHz NMR spectrometer with 5 mm BBFO probe). Deuterated chloroform ($CDCl_3$, Euriso-top, 99.8%), and deuterated water (D_2O, Euri-so-top,

99.8%) were used as solvents and references for the lock. Bruker Topspin Software was used for data treatment.

Size Exclusion Chromatography (SEC): Measurements in DMSO were performed on an Ultimate 3000 system from Thermoscientific equipped with a diode array detector (DAD). The system also include a multi-angles light scattering detector (MALS) and differential refractive index detector (dRI) from Wyatt technology. Polymers were separated on Tosoh TSK G3000HHR and G2000HHR (7.8*300) columns (exclusion limits from 200 Da to 60 000 Da) at a flowrate of 0.5 mL min^{-1}. Columns temperatures were maintained at 80 °C. Dextran from PSS was used as the standard. Dimethysulfoxide (DMSO + lithium bromide LiBr 1 g L^{-1}) was used as the eluent.

Sodium dodecyl sulfate – polyacrylamide gel electrophoresis (SDS-PAGE) analysis: 10 μL of Precision Plus ProteinTM Standards (BIO-RAD, un-stained) was used as size marker. 15 μL of sample were loaded in gel wells (BIO-RAD, 4–20% Mini-PROTEAN® TGX™ stain-free gel). Tris-Glycine-SDS Buffer (BIO-RAD, TGS 1x) was used as loading buffer. Laemmli Sample Buffer (BIO-RAD, 2x) was used as a running buffer.

Matrix-assisted laser desorption/ionization mass spectrometry (MALDI MS): MALDI-MS spectra were performed by the CESAMO (Bordeaux, France) on an Autoflex maX TOF mass spectrometer (Bruker Daltonics, Bremen, Germany) equipped with a frequency tripled Nd:YAG laser emitting at 355 nm. Spectra were recorded in the linear positive-ion mode with an accelerating voltage of 19 kV. Samples were dissolved in water at 4 mg mL^{-1}. The SA matrix (sinapinic acid) solution was prepared by dissolving 10 mg in 1 mL of acetonitrile/0.1% aqueous TFA 50/50. The solutions were combined in a 10:10 volume ratio of matrix to sample.

One to two microliters of the obtained solution was deposited onto the sample target and vacuum-dried.

Matrix-assisted laser desorption/ionization time of flight (MALDI-TOF): MALDI-TOF spectra were recorded using an AXIMA Confidence Shimadzu spectrometer, using trans-2-[3-(4-tert-Butylphenyl)-2-methyl-2-propenylidene]malononitrile (DCTB) as a matrix.

UV-Vis spectroscopy: The transition temperatures ($T_{CP,}$ cloud point) were determined by following the turbidity at 600 and 500 nm absorption versus temperature on Agilent Cary 100 UV-Vis spectrophotometer equipped with a multicell thermo-electric temperature controller. Turbidity has been measured over a temperature range from 10 to 65 °C at 1 °C min^{-1} of a scan rate before and after the TT1 conjugation at three concentrations (10, 20 and 30 μM) in phosphate buffer (PBS, pH 7.4). The T_{CP} corresponds to the onset temperature where the absorbance starts increasing.

Dynamic light scattering: The DLS measurements of *TT1*-ELP[M_1V_3-*40*] and *TT1*-ELP[$M(O)_1V_3$-*40*] were performed on NanoZS 90 instrument (HeNe laser 632.8 nm, Malvern, U.K.) at a 90° angle at a constant position in the cuvette (constant scattering volume at 30 μM concentration in 1x PBS, pH 7.4). The values of Z-average hydrodynamic diameter (D_H) obtained from the 2nd order cumulant fit using a CONTIN-like algorithm. The T_{CP} measured by DLS temperature ramp (10-55 °C) correspond to the onset temperature where the size and DCR starts increasing.

Atomic Force Microscopy (AFM): Temperature-controlled liquid atomic force microscopy measurements were performed using a Dimension Fast Scan Bruker AFM system. The topography images of the bioconjugates were obtained in Peak Force tapping mode, using a

Silicon cantilever (ScanAsyst-Fluid+, Bruker) with a typical tip radius of 5 nm. The cantilever resonance was 150 kHz and the spring constant was 0.7 N m^{-1}. Samples were prepared by drop-casting a bioconjugates solution of 50 μM onto a freshly cleaved mica or HOPG surface purchased from Agar Scientific, which was directly applied for imaging. AFM imaging process was achieved in the liquid environment at specific temperature. An external heating stage (Bruker) was used to achieve the target temperature at the substrate surface.

Photo-irradiation experiment: 3 mg of *TT1*-ELP[M_1V_3-*40*] was dissolved in 0.5 mL of D_2O and transferred to the NMR tube. ^{1}H NMR spectra has been taken before and after every 5 min during 30 min of the LED (Luzchem LEDi, red region 630-640 nm, irradiance >2100 W/m^2) irradiation to monitor the photooxidation of the methionine residue at ambient temperature *via* 200 MHz ^{1}H NMR.

Acknowledgements

Financial support from EuroNanoMed3 (2017-191, TEMPEAT), SIRIC BRIO (INCA, COMMUCAN project), and Spanish MICINN (T.T.) (CTQ2017-85393-P and PCIN-2017-042) are gratefully acknowledged. IMDEA Nanociencia acknowledges support from the "Severo Ochoa" Program for Centers of Excellence in R&D (MINECO, Grant SEV2016-0686). We gratefully acknowledge Gilles Pecastaings, Amelie Vax and Anne-Laure Wirotius from LCPO for liquid-AFM, SEC and NMR analysis, respectively and Christelle Absalon from CESAMO for MALDI analysis. J.A.G.D. thanks the Government of Spain for a Juan de la Cierva fellowship. Arnaud Tron and Dr. Nathan D. McClenaghan from ISM, Unversity of Bordeaux are gratefully acknowledged for providing Luzchem LEDi device to evaluate the photooxidation process.

Abbreviations

PDT, photodynamic therapy; PS, photosensitizer; ELP, elastin like polypeptide; IPT, inverse phase transition; T_t, transition temperature; ITC, inverse transition cycling; EPR, enhanced permeability and retention effect; TT1, Zn(II)-phthalocyanine, [*9(10),16(17),23(24)-Tri-tert-butyl-2-carboxy-5,28:14,19-diimino-7,12:21,26-dinitrilotetrabenzo[c,h,m,r][1,6,11,16]tetraazacycloeicosinato-(2$^-$)-N^{29},N^{30},N^{31},N^{32} zinc* (II) (mixture of regioisomers)].

References

1. Allison, R. R.; Sibata C. H., Oncologic photodynamic therapy photosensitizers: A clinical review *Photodiagnosis and Photodynamic Therapy* **2010**, *7*, 61-75.

2. Hackbarth, S.; Islam, W.; Fang, J.; Šubr, V.; Röder, B.; Etrych, T.; Maeda, H., Singlet oxygen phosphorescence detection in vivo identifies PDT-induced anoxia in solid tumors. *Photochemical & Photobiological Sciences* **2019,** *18* (6), 1304-1314.

3. Lukyanets, E. A., Phthalocyanines as Photosensitizers in the Photodynamic Therapy of Cancer. *Journal of Porphyrins and Phthalocyanines* **1999,** *3* (6), 424-432.

4. Brancaleon, L.; Moseley, H., Laser and Non-laser Light Sources for Photodynamic Therapy. *Lasers in Medical Science* **2002,** *17* (3), 173-186.

5. Moor, A. C. E.; Ortel, B.; Hasan, T., Mechanisms of photodynamic therapy. In *Photodynamic Therapy*, Patrice, T., Ed. The Royal Society of Chemistry **2003**, *2*, 19-58.

6. Hsieh, Y. J.; Chien, K. Y.; Lin, S. Y.; Sabu, S.; Hsu, R. M.; Chi, L. M.; Lyu, P. C.; Yu, J. S., Photofrin binds to procaspase-3 and mediates photodynamic treatment-triggered methionine oxidation and inactivation of procaspase-3. *Cell Death &Amp; Disease* **2012,** *3*, e347-358.

7. Gollnick, S. O.; Evans, S. S.; Baumann, H.; Owczarczak, B.; Maier, P.; Vaughan, L.; Wang, W. C.; Unger, E.; Henderson, B. W., Role of cytokines in photodynamic therapy-induced local and systemic inflammation. *British Journal of Cancer* **2003,** *88* (11), 1772-1779.

8. Castano, A. P.; Mroz, P.; Hamblin, M. R., Photodynamic therapy and anti-tumour immunity. *Nature Reviews Cancer* **2006,** *6* (7), 535-545.

9. Kamkaew, A.; Lim, S. H.; Lee, H. B.; Kiew, L. V.; Chung, L. Y.; Burgess, K., BODIPY dyes in photodynamic therapy. *Chemical Society Reviews* **2013,** *42* (1), 77-88.

10. Li, X.; Zheng, B.-D.; Peng, X.-H.; Li, S.-Z.; Ying, J.-W.; Zhao, Y.; Huang, J.-D.; Yoon, J., Phthalocyanines as medicinal photosensitizers: Developments in the last five years. *Coordination Chemistry Reviews* **2019,** *379*, 147-160.

11. Brasseur, N., Sensitizers for PDT: phthalocyanines. In *Photodynamic Therapy*, Patrice, T., Ed. The Royal Society of Chemistry **2003**, *2*, 105-118.

12. Almeida-Marrero, V.; Van de Winckel, E.; Anaya-Plaza, E.; Torres, T.; de la Escosura, A., Porphyrinoid biohybrid materials as an emerging toolbox for biomedical light management. *Chemical Society Reviews* **2018,** *47* (19), 7369-7400.

13. Lo, P.-C.; Rodríguez-Morgade, M. S.; Pandey, R. K.; Ng, D. K. P.; Torres, T.; Dumoulin, F., The unique features and promises of phthalocyanines as advanced photosensitisers for photodynamic therapy of cancer. *Chemical Society Reviews* **2020,** *49* (4), 1041-1056.

14. Ferreira, J. T.; Pina, J.; Ribeiro, C. A. F.; Fernandes, R.; Tomé, J. P. C.; Rodríguez-Morgade, M. S.; Torres, T., Highly Efficient Singlet Oxygen Generators Based on Ruthenium Phthalocyanines: Synthesis, Characterization and in vitro Evaluation for Photodynamic Therapy. *Chemistry – A European Journal* **2020,** *26* (8), 1789-1799.

15. (a) Ogunsipe, A.; Nyokong, T., Effects of central metal on the photophysical and photochemical properties of non-transition metal sulfophthalocyanine. *Journal of Porphyrins and Phthalocyanines* **2005,** *09* (02), 121-129; (b) Mwanza, D.; Louzada, M.; Britton, J.; Sekhosana, E.; Khene, S.; Nyokong, T.; Mashazi, P., The effect of the cobalt and manganese central metal ions on the nonlinear optical properties of tetra(4-propargyloxyphenoxy)phthalocyanines. *New Journal of Chemistry* **2018,** *42* (12), 9857-9864.

16. Ageitos, J. M.; Chuah, J.-A.; Numata, K., Chapter 1 Design Considerations for Properties of Nanocarriers on Disposition and Efficiency of Drug and Gene Delivery. In

Nanomedicines: Design, Delivery and Detection, The Royal Society of Chemistry **2016**, 1-22.

17. Van der Meel, R.; Sulheim, E.; Shi, Y.; Kiessling, F.; Mulder, W. J. M.; Lammers, T., Smart cancer nanomedicine. *Nature Nanotechnology* **2019,** *14* (11), 1007-1017.

18. Ibrahimova, V.; Denisov, S. A.; Vanvarenberg, K.; Verwilst, P.; Préat, V.; Guigner, J.-M.; McClenaghan, N. D.; Lecommandoux, S.; Fustin, C.-A., Photosensitizer localization in amphiphilic block copolymers controls photodynamic therapy efficacy. *Nanoscale* **2017,** *9* (31), 11180-11186.

19. MacEwan, S. R.; Chilkoti, A., Elastin-like polypeptides: Biomedical applications of tunable biopolymers. *Peptide Science* **2010,** *94* (1), 60-77.

20. Rodríguez-Cabello, J. C.; Arias, F. J.; Rodrigo, M. A.; Girotti, A., Elastin-like polypeptides in drug delivery. *Advanced Drug Delivery Reviews* **2016,** *97*, 85-100.

21. Urry, D. W.; Physical Chemistry of Biological Free Energy Transduction As Demonstrated by Elastic Protein-Based Polymers. *J. Phys. Chem. B* **1997**, *101* (51), 11007–11028.

22. Petitdemange, R.; Garanger, E.; Bataille, L.; Dieryck, W.; Bathany, K.; Garbay, B.; Deming, T. J.; Lecommandoux, S., Selective Tuning of Elastin-like Polypeptide Properties via Methionine Oxidation. *Biomacromolecules* **2017,** *18* (2), 544-550.

23. Aluri, S.; Pastuszka, M. K.; Moses, A. S.; MacKay, J. A., Elastin-Like Peptide Amphiphiles Form Nanofibers with Tunable Length. *Biomacromolecules* **2012,** *13* (9), 2645-2654.

24. Mozhdehi, D.; Luginbuhl, K. M.; Simon, J. R.; Dzuricky, M.; Berger, R.; Varol, H. S.; Huang, F. C.; Buehne, K. L.; Mayne, N. R.; Weitzhandler, I. *et al.*, Genetically encoded lipid–polypeptide hybrid biomaterials that exhibit temperature-triggered hierarchical self-assembly. *Nature Chemistry* **2018,** *10* (5), 496-505.

25. Petitdemange, R.; Garanger, E.; Bataille, L.; Bathany, K.; Garbay, B.; Deming, T. J.; Lecommandoux, S., Tuning Thermoresponsive Properties of Cationic Elastin-like Polypeptides by Varying Counterions and Side-Chains. *Bioconjugate Chemistry* **2017,** *28* (5), 1403-1412.

26. Kramer, J. R.; Petitdemange, R.; Bataille, L.; Bathany, K.; Wirotius, A.-L.; Garbay, B.; Deming, T. J.; Garanger, E.; Lecommandoux, S., Quantitative Side-Chain Modifications of Methionine-Containing Elastin-Like Polypeptides as a Versatile Tool to Tune Their Properties. *ACS Macro Lett*. **2015**, *4*, 1283–1286

27. Xiao, Y.; Chinoy, Z. S.; Pecastaings, G.; Bathany, K.; Garanger, E.; Lecommandoux, S., Design of Polysaccharide-b-Elastin-Like Polypeptide Bioconjugates and Their Thermoresponsive Self-Assembly. *Biomacromolecules* **2020**, *21*, 114-125.

28. Rosselin, M.; Xiao, Y.; Belhomme, L.; Lecommandoux, S.; Garanger, E., Expanding the Toolbox of Chemoselective Modifications of Protein-Like Polymers at Methionine Residues. *ACS Macro Letters* **2019**, 1648-1653.

29. Bravo-Anaya, L. M.; Garbay, B.; Nando-Rodríguez, J. L. E.; Carvajal Ramos, F.; Ibarboure, E.; Bathany, K.; Xia, Y.; Rosselgong, J.; Joucla, G.; Garanger, E. *et al.*, Nucleic acids complexation with cationic elastin-like polypeptides: Stoichiometry and stability of nano-assemblies. *Journal of Colloid and Interface Science* **2019,** *557*, 777-792.

30. Anaya, L. M. B.; Petitdemange, R.; Rosselin, M.; Ibarboure, E.; Garbay, B.; Garanger, E.; Deming, T. J.; Lecommandoux, S., Design of Thermoresponsive Elastin-Like Glycopolypeptides for Selective Lectin Binding and Sorting. *Biomacromolecules* **2020,** *22* (1), 76-85.

31. Cid, J.-J.; Yum, J.-H.; Jang, S.-R.; Nazeeruddin, M. K.; Martínez-Ferrero, E.; Palomares, E.; Ko, J.; Grätzel, M.; Torres, T., Molecular Cosensitization for Efficient Panchromatic Dye-Sensitized Solar Cells. *Angewandte Chemie International Edition* **2007,** *46* (44), 8358-8362.

32. Ylä-Herttuala, S.; Christensen, J. B.; Moghimi, S.M.; Torres Cebada, T.; Trohopoulos, P. N.; Makinen, P.; Ficker, M.; Wu, L.; Medel Gonzalez, M., Nano-systems for therapy and/or diagnosis and/or therapy Monitoring and/or theranostics of disease, PCT/EP 16168476.6., 05/05/2016.

33. Aktas, E.; Jiménez-López, J.; Azizi, K.; Torres, T.; Palomares, E., Self-assembled Zn phthalocyanine as a robust p-type selective contact in perovskite solar cells. *Nanoscale Horizons* **2020**, *5*, 1415-1419

34. Meyer, D. E.; Chilkoti, A., Purification of recombinant proteins by fusion with thermally-responsive polypeptides. *Nature Biotechnology* **1999,** *17* (11), 1112-1115.

35. Ye, C.; Zhang, Y.; Ding, A.; Hu, Y.; Guo, H., Visible light sensitizer-catalyzed highly selective photo oxidation from thioethers into sulfoxides under aerobic condition. *Scientific Reports* **2018,** *8* (1), 2205-2211.

36. Kim, H.-Y.; Gladyshev, Vadim N., Methionine sulfoxide reductases: selenoprotein forms and roles in antioxidant protein repair in mammals. *Biochemical Journal* **2007,** *407* (3), 321-329.

37. Meyer, D. E.; Chilkoti, A., Genetically Encoded Synthesis of Protein-Based Polymers with Precisely Specified Molecular Weight and Sequence by Recursive Directional Ligation: Examples from the Elastin-like Polypeptide System. *Biomacromolecules* **2002,** *3* (2), 357-367.

38. Le, D. H. T.; Sugawara-Narutaki, A., Elastin-like polypeptides as building motifs toward designing functional nanobiomaterials. *Molecular Systems Design & Engineering* **2019,** *4* (3), 545-565.

39. Schüder, G.; Pistorius, G.; Fehringer, M.; Feifel, G.; Menger, M. D.; Vollmar, B., Complete shutdown of microvascular perfusion upon hepatic cryothermia is critically dependent on local tissue temperature. *British Journal of Cancer* **2000,** *82* (4), 794-799.

40. Ibáñez-Fonseca, A.; Santiago Maniega, S.; Gorbenko del Blanco, D.; Catalán Bernardos, B.; Vega Castrillo, A.; Álvarez Barcia, Á. J.; Alonso, M.; Aguado, H. J.; Rodríguez-Cabello, J. C., Elastin-Like Recombinamer Hydrogels for Improved Skeletal Muscle Healing Through Modulation of Macrophage Polarization. *Frontiers in Bioengineering and Biotechnology* **2020**, *8*, 413-424.

41. McDaniel, J. R.; Callahan, D. J.; Chilkoti, A., Drug delivery to solid tumors by elastin-like polypeptides. *Adv. Drug Deliv. Rev.* **2010**, *62* (15), 1456-1467.

42. Manzari, M. T.; Anderson, G. R.; Lin, K. H.; Soderquist, R. S.; Çakir, M.; Zhang, M.; Moore, C. E.; Skelton, R. N.; Fèvre, M., Li, X. *et al.*, Genomically informed small-molecule drugs overcome resistance to a sustained-release formulation of an engineered

death receptor agonist in patient-derived tumor models. *Sci. Adv.* **2019**, *5* (9), eaaw9162-9176.

Author manuscript of article published in Bioconjugate Chemistry (2021) https://doi.org/10.1021/acs.bioconjchem.1c00251

Photooxidation Responsive Elastin-Like Polypeptide Conjugates for Photodynamic Therapy Application

Vusala Ibrahimova,[†] José A. González-Delgado,[‡] Manon Levêque,[†] Tomas Torres,*[‡, ǁ, §] Elisabeth Garanger,*[†] and Sébastien Lecommandoux*[†]

[†] Univ. Bordeaux, CNRS, Bordeaux INP, LCPO, UMR 5629, F-33600, Pessac, France

[‡] Departamento de Química Orgánica, Universidad Autónoma de Madrid, 28049 Madrid, Spain

[ǁ] IMDEA-Nanociencia, Campus de Cantoblanco, 28049 Madrid, Spain

[§] Institute for Advanced Research in Chemical Sciences (IAdChem), Universidad Autónoma de Madrid, 28049 Madrid, Spain

Corresponding authors: lecommandoux@enscbp.fr; garanger@enscbp.fr; tomas.torres@uam.es

TT1-amide-C3-azide (1)

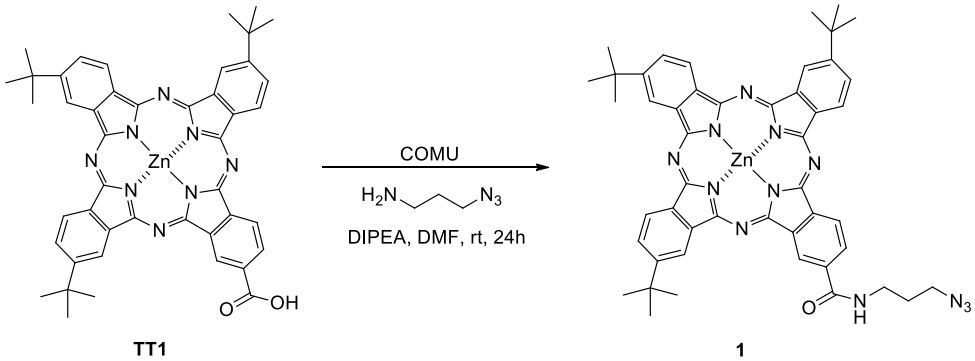

Scheme S1. Synthesis of TT1-amide-C3-azide (**1**).

Reagents: *9(10),16(17),23(24)-Tri-tert-butyl-2-carboxy-5,28:14,19-diimino-7,12:21,26-dinitrilo-tetrabenzo[c,h,m,r][1,6,11,16]tetraazacycloeicosinato-(2⁻)-N^{29},N^{30},N^{31},N^{32} zinc* (II)

(mixture of regioisomers) (**TT1**), 3-azidopropylamine ($C_3H_8N_4$, TCI Europe, >95.0%), COMU® ($C_{12}H_{19}F_6N_4O_4P$, Sigma-Aldrich, 97%)

Solvents: 1,4-dioxane (HPLC - Stabilized with BHT, Carlo Erba), n-hexane (99% for analysis, Carlo Erba)

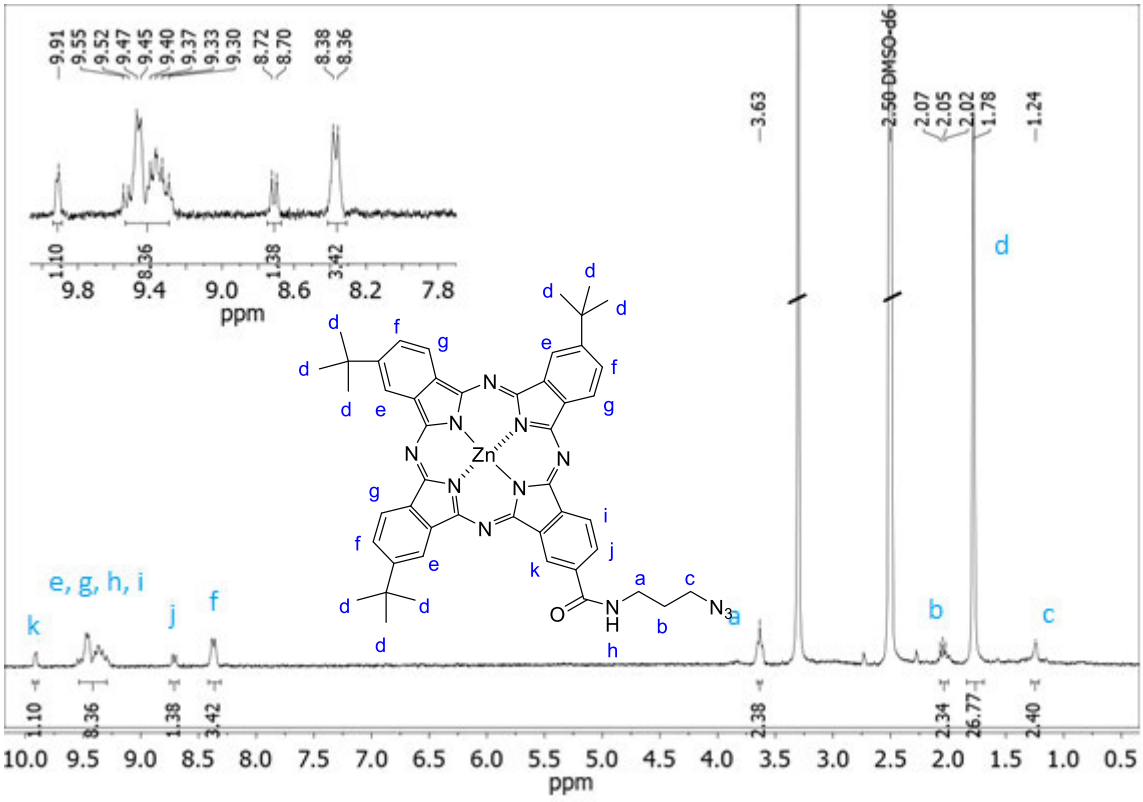

Figure S1. ^{1}H NMR spectrum of TT1-amide-C3-azide (**1**) (DMSO-d_6).

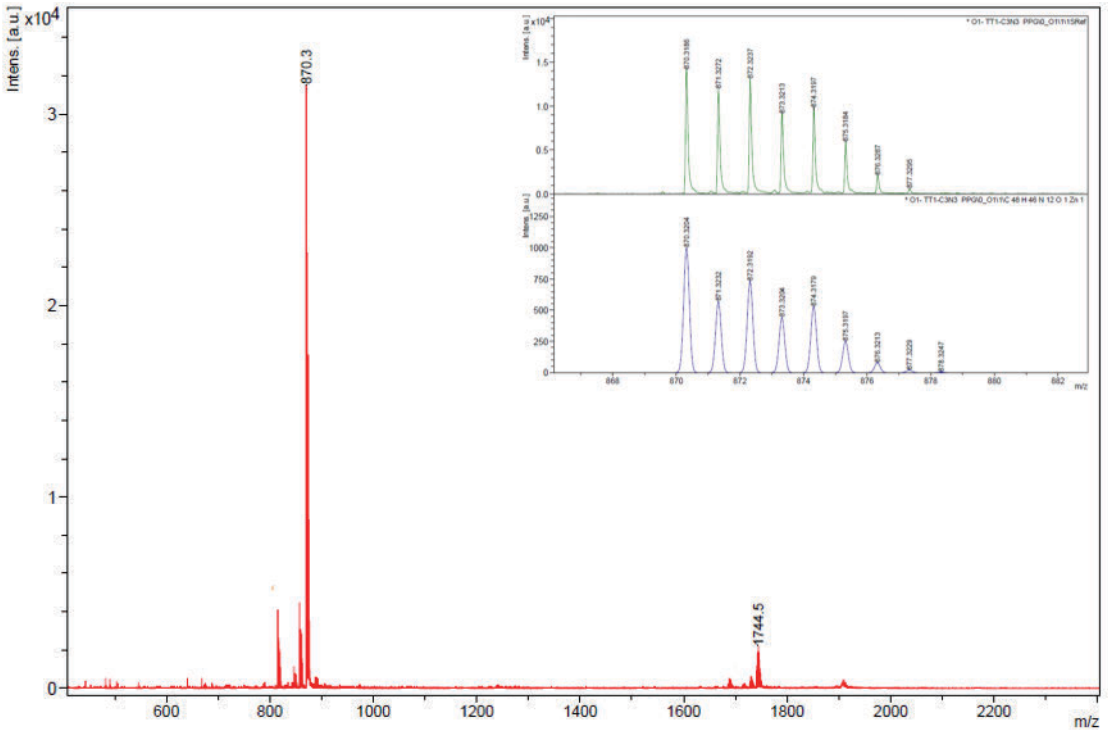

Figure S2. MS and HRMS (MALDI-TOF, DCTB) of TT1-amide-C3-azide (**1**)

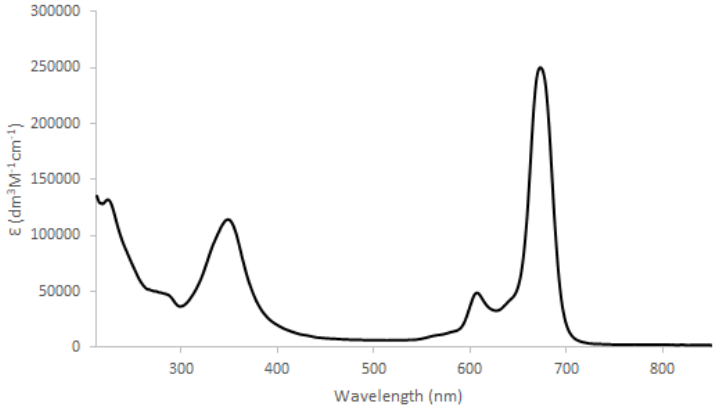

Figure S3. UV-Vis spectrum of TT1-amide-C3-azide (**1**) in THF (Concentration $2{,}14 \cdot 10^{-6}$ M).

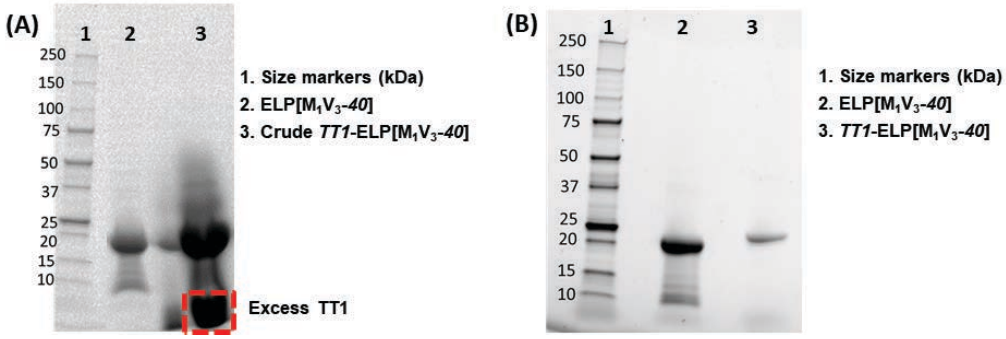

Figure S4. SDS-PAGE analysis of *TT1*-ELP[M_1V_3-*40*] (A) before and (B) after purification.

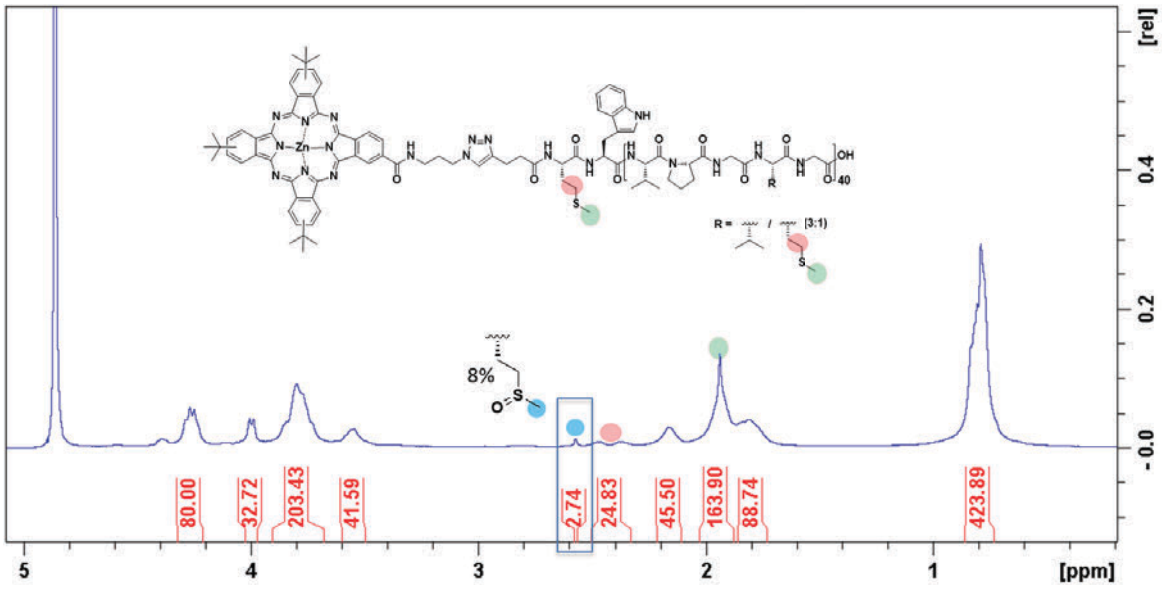

Figure S5. ^{1}H NMR spectrum of *TT1*-ELP[M_1V_3-*40*] in D_2O at 5 °C.

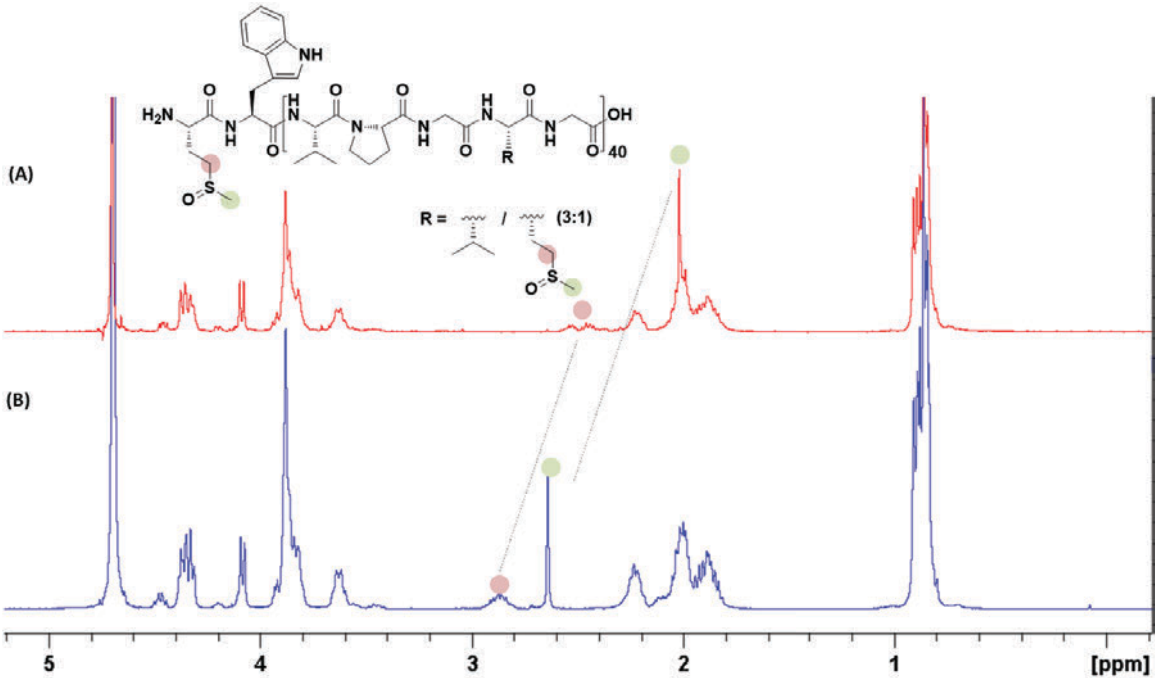

Figure S6. ^{1}H NMR spectrum of ELP[M(O)$_1$V$_3$-*40*], (A) before and (B) after the chemical oxidation, in D_2O at room temperature.

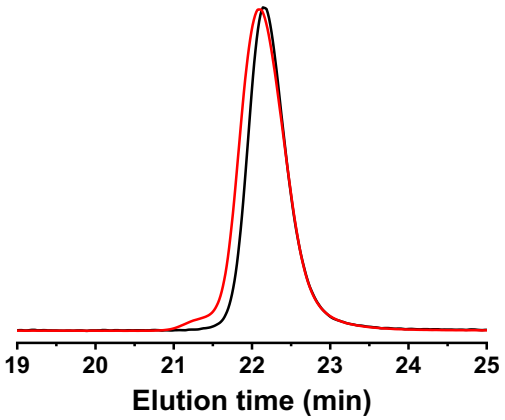

Figure S7. Size exclusion chromatograms (RI detection) in DMSO of ELP[M$_1$V$_3$-*40*] (black curve) and ELP[M(O)$_1$V$_3$-*40*] (red curve).

N-terminal modification of ELP[M(O)$_1$V$_3$-40]

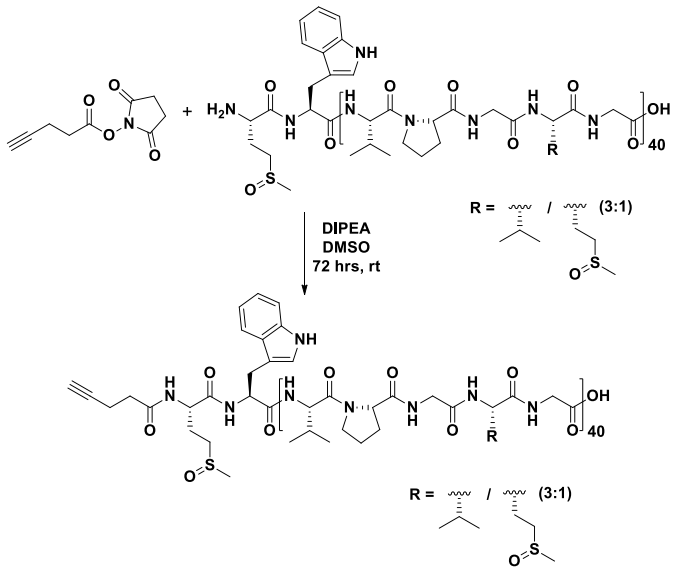

Scheme S2. Synthesis of *Alkyne*-ELP[M(*O*)$_1$V$_3$-*40*].

To a solution of ELP[M(*O*)$_1$V$_3$-*40*] (40 mg, 2.32 μmol) in anhydrous DMSO (2 mL) *N, N*-diisopropylethylamine (0.3 mg, 2.32 μmol) was added and followed by addition of 4-pentynoic acid succinimidyl ester (9 mg, 46.48 μmol). The reaction mixture was stirred for 72h under Ar at room temperature. Then the solution was diluted with 15 mL of water and dialyzed against ultrapure water in a dialysis bag (cut-off MWCO 3.5 kDa) for 72h by changing the water every 3h. The solution was lyophilized to yield *Alkyne*-ELP[M(*O*)$_1$V$_3$-*40*] (30 mg, 75%) as a white powder.

^{1}H NMR (400 MHz, D_2O, 25 °C): δ 4.29−4.23 (m, 80 H, αC*H* Val, Pro), 4.09−3.99 (d, 30 H, αC*H* VPGVG), 2.85−2.73 (m, 22 H, CH_2S Met), 2.38-2.29 (br m, γCH_2 Met, $CH_2CH_2C{\equiv}CH$), 2.56 (s, 33 H, SCH_3 Met), 0.82−0.75 (br m, 420 H, CH_3 Val).

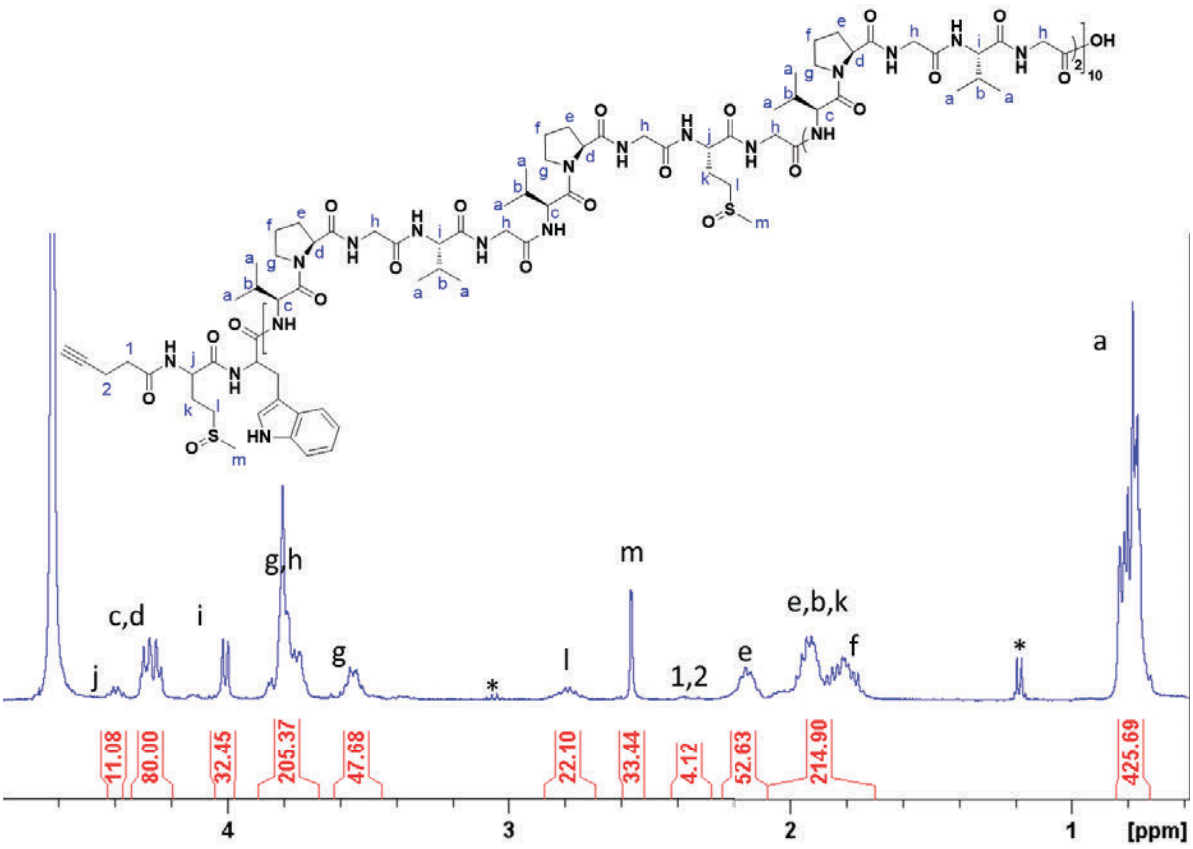

Figure S8. ^{1}H NMR spectrum of *Alkyne*-ELP[M(O)$_1$V$_3$-*40*] in D_2O at room temperature (*EtOH).

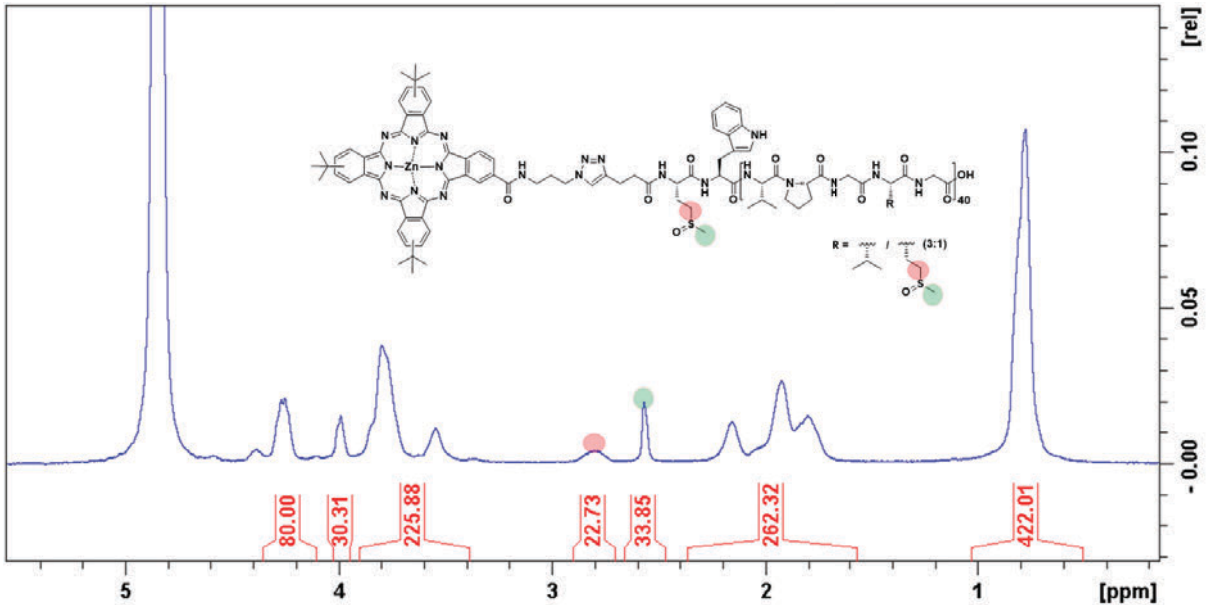

Figure S9. ^{1}H NMR spectrum of *TT1*-ELP[M(O)$_1$V$_3$-*40*] in D_2O at 5 °C.

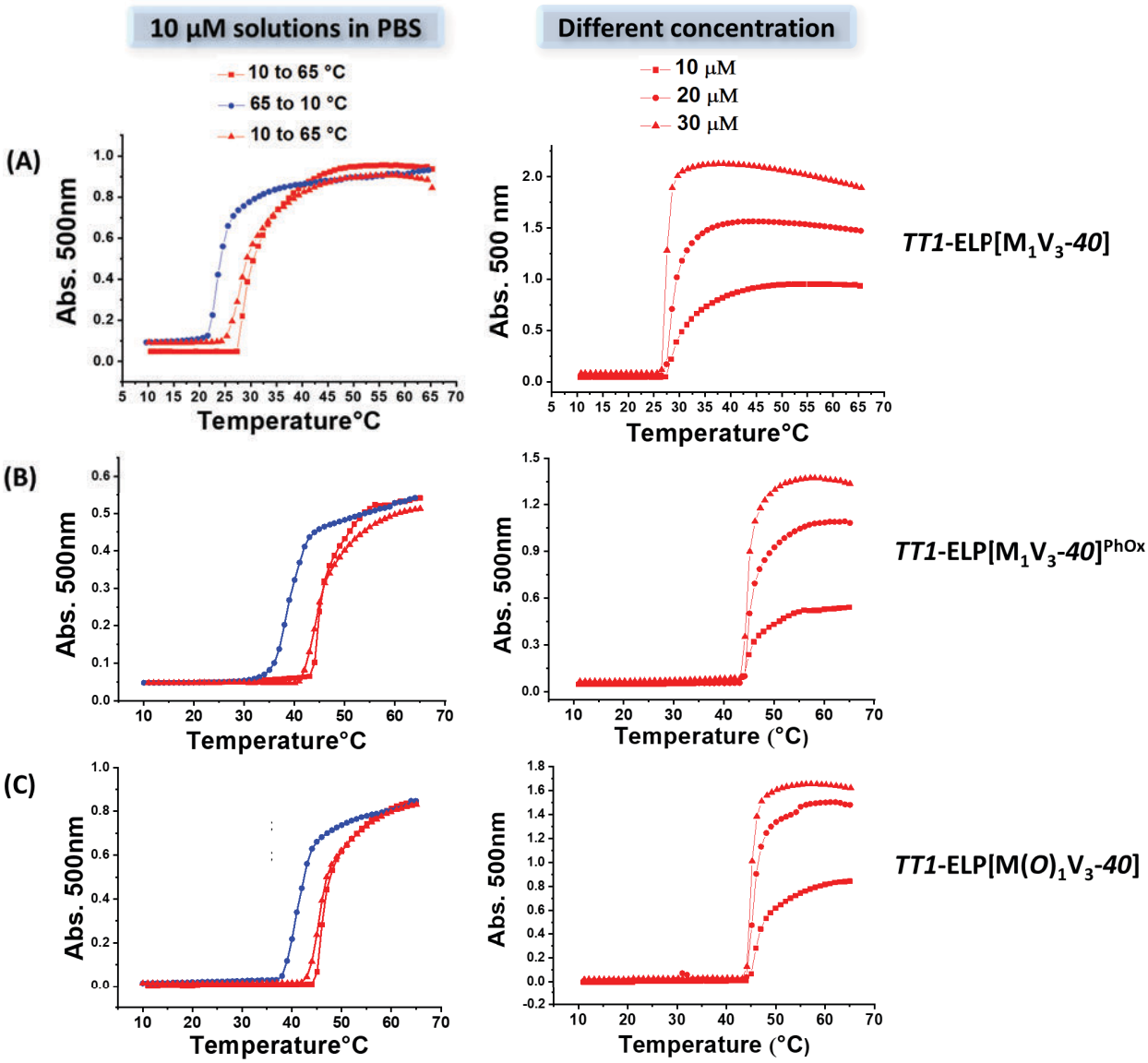

Figure S10. Absorbance (A.U.) at 500 nm of (A) *TT1*-ELP[M_1V_3-*40*], (B) *TT1*-ELP[M_1V_3-*40*] photooxidized, noted *TT1*-ELP[M_1V_3-*40*]^{PhOx}, and (C) *TT1*-ELP[M(*O*)$_1V_3$-*40*] solutions upon heating-cooling-heating (10-65 °C) cycles at 10 µM (left panels) and upon heating at 10 µM, 20 µM and 30 µM concentrations (right panels) in PBS as a function of temperature.

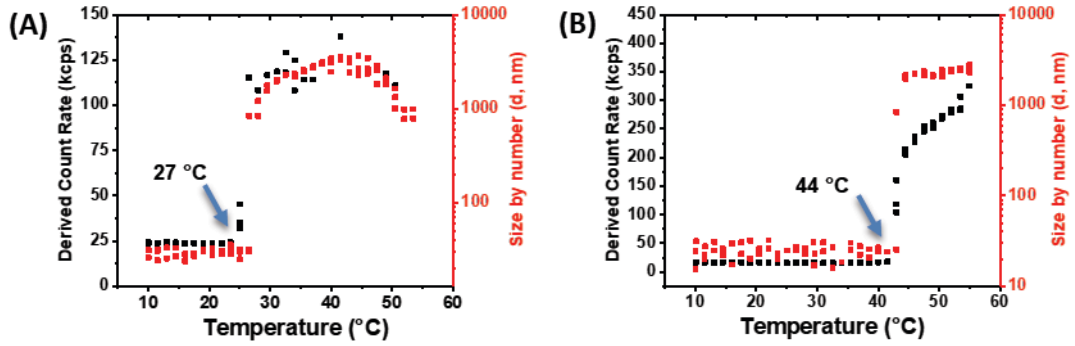

Figure S11. Temperature ramp results of (A) *TT1*-ELP[M_1V_3-*40*] and (B) *TT1*-ELP[$M(O)_1V_3$-*40*] solutions at 30 μM concentration in PBS buffer upon heating at a range of 10-55 °C (1.5 °C step, n=3) measured by DLS at 90° angle.

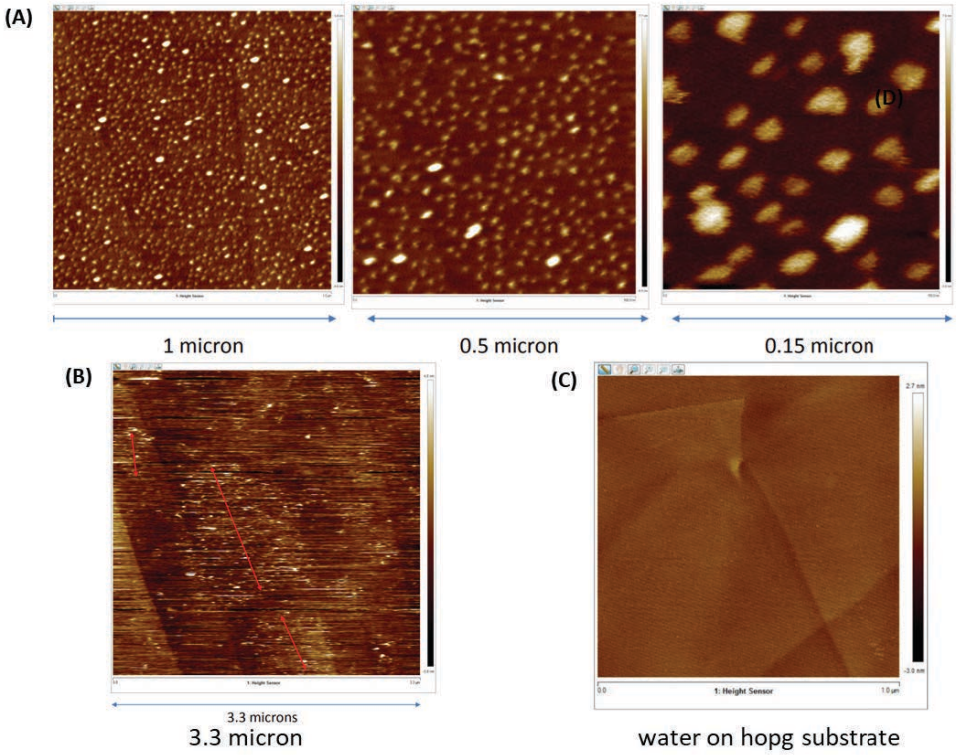

Figure S12. Temperature-Controlled High-Speed AFM (liquid) images of *TT1*-ELP[M_1V_3-*40*] on HOPG substrate (A) at 15 °C, (B) at 50 °C in PBS and (C) pure water on HOPG substrate.

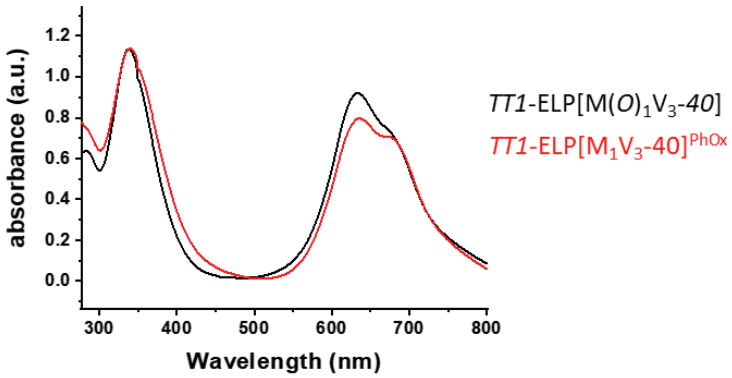

Figure S13. Overlapped absorption spectra of *TT1*-ELP[$M(O)_1V_3$-*40*] (black curve) and *TT1*-ELP[M_1V_3-*40*]^{PhOx} (red curve) in water.

Photooxidation Responsive Elastin-Like Polypeptide Conjugates for Photodynamic Therapy Application

Vusala Ibrahimova,[†] José A. González-Delgado,[‡] Manon Levêque,[†] Tomas Torres,*[‡, ǁ, §] Elisabeth Garanger,*[†] and Sébastien Lecommandoux*[†]

[†] Univ. Bordeaux, CNRS, Bordeaux INP, LCPO, UMR 5629, F-33600, Pessac, France

[‡] Departamento de Química Orgánica, Universidad Autónoma de Madrid, 28049 Madrid, Spain

[ǁ] IMDEA-Nanociencia, Campus de Cantoblanco, 28049 Madrid, Spain

[§] Institute for Advanced Research in Chemical Sciences (IAdChem), Universidad Autónoma de Madrid, 28049 Madrid, Spain

Corresponding authors: lecommandoux@enscbp.fr; garanger@enscbp.fr; tomas.torres@uam.es

TT1-amide-C3-azide (1)

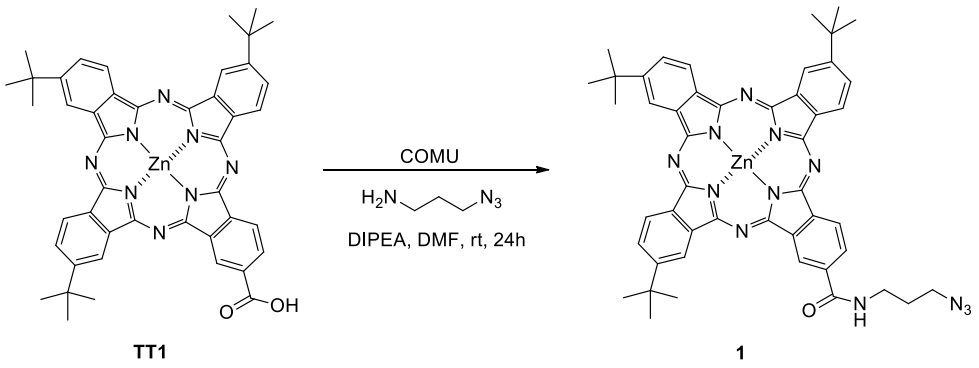

Scheme S1. Synthesis of TT1-amide-C3-azide (**1**).

Reagents: *9(10),16(17),23(24)-Tri-tert-butyl-2-carboxy-5,28:14,19-diimino-7,12:21,26-dinitrilo-tetrabenzo[c,h,m,r][1,6,11,16]tetraazacycloeicosinato-(2⁻)-N^{29},N^{30},N^{31},N^{32} zinc* (II) (mixture of regioisomers) (**TT1**), 3-azidopropylamine ($C_3H_8N_4$, TCI Europe, >95.0%), COMU® ($C_{12}H_{19}F_6N_4O_4P$, Sigma-Aldrich, 97%)

Solvents: 1,4-dioxane (HPLC - Stabilized with BHT, Carlo Erba), n-hexane (99% for analysis, Carlo Erba)

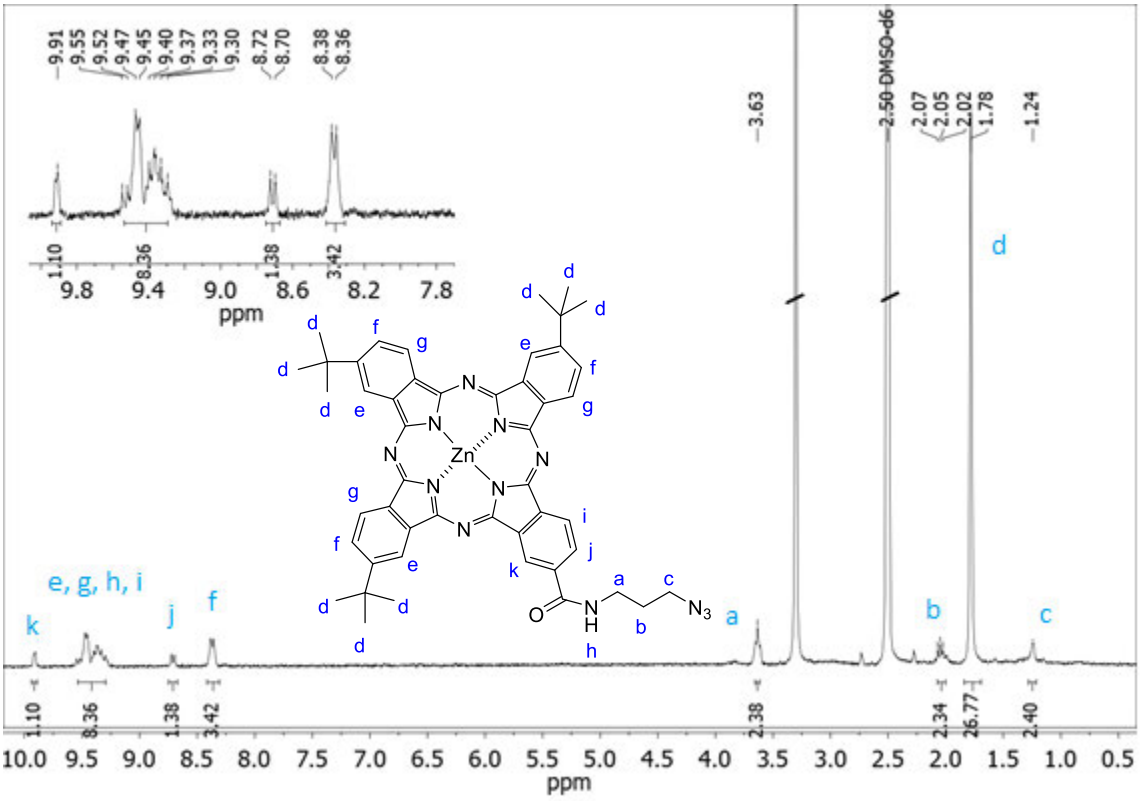

Figure S1. ^{1}H NMR spectrum of TT1-amide-C3-azide (**1**) (DMSO-d_6).

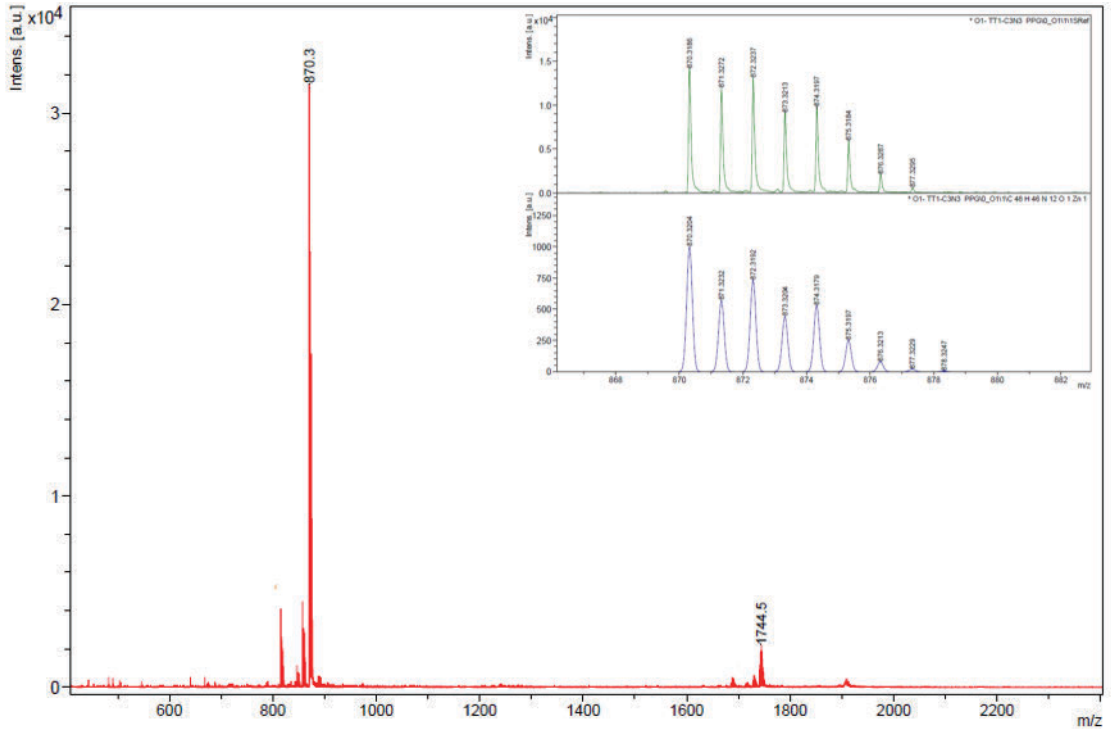

Figure S2. MS and HRMS (MALDI-TOF, DCTB) of TT1-amide-C3-azide (**1**)

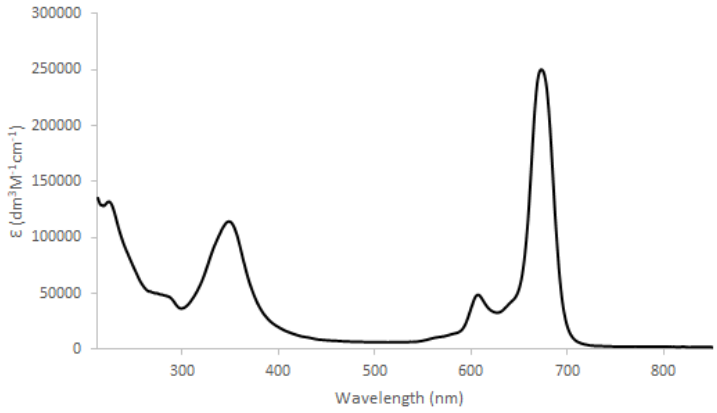

Figure S3. UV-Vis spectrum of TT1-amide-C3-azide (**1**) in THF (Concentration $2{,}14 \cdot 10^{-6}$ M).

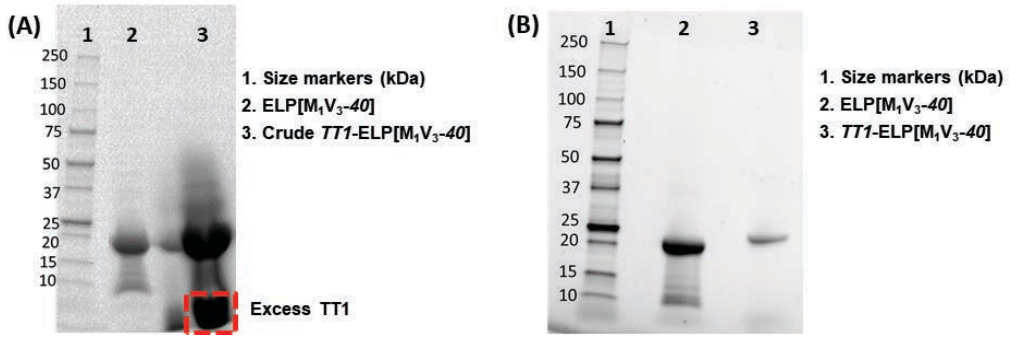

Figure S4. SDS-PAGE analysis of *TT1*-ELP[M_1V_3-*40*] (A) before and (B) after purification.

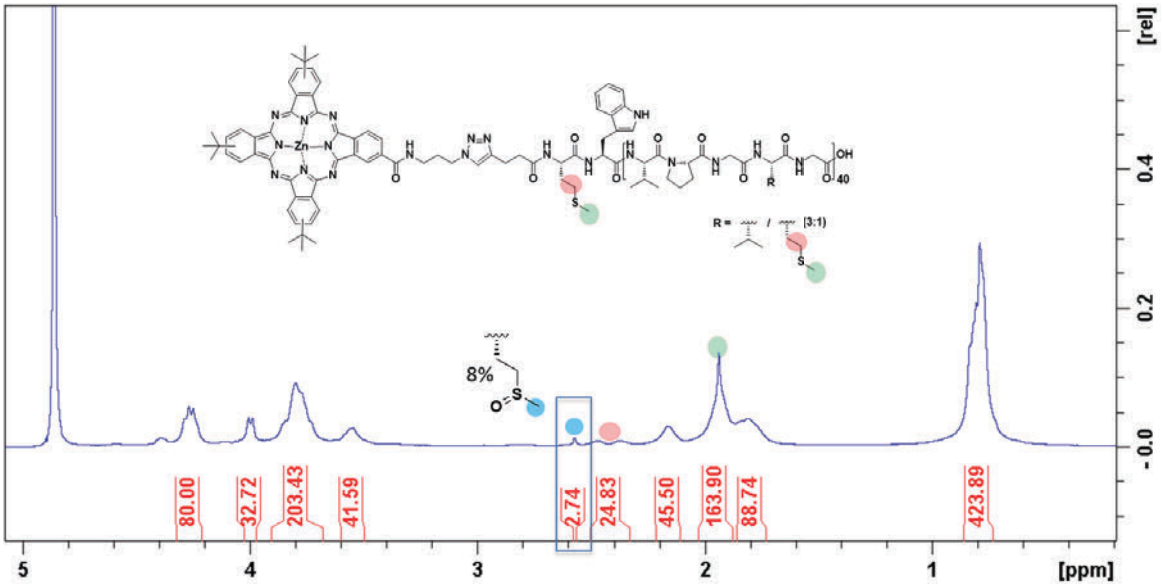

Figure S5. ^{1}H NMR spectrum of *TT1*-ELP[M_1V_3-*40*] in D_2O at 5 °C.

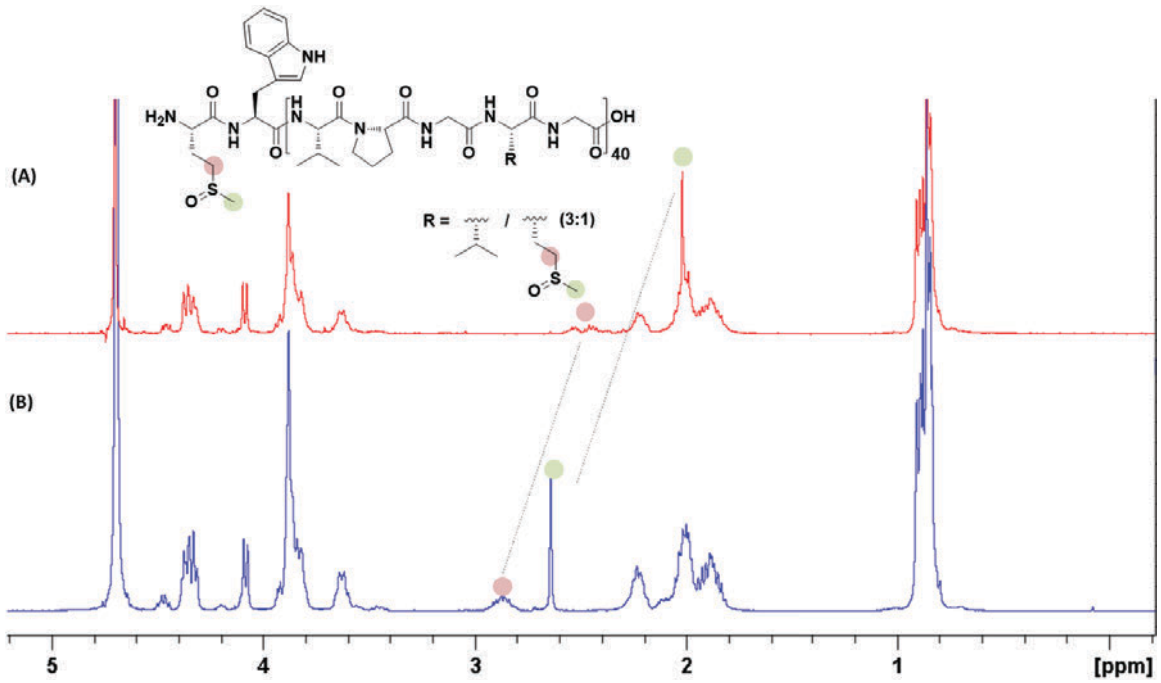

Figure S6. ^{1}H NMR spectrum of ELP[M(O)$_1$V$_3$-*40*], (A) before and (B) after the chemical oxidation, in D_2O at room temperature.

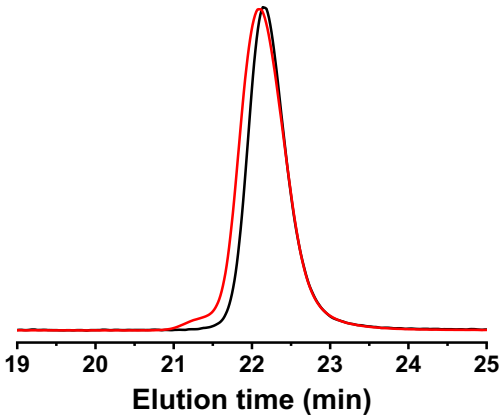

Figure S7. Size exclusion chromatograms (RI detection) in DMSO of ELP[M$_1$V$_3$-*40*] (black curve) and ELP[M(O)$_1$V$_3$-*40*] (red curve).

N-terminal modification of ELP[M(O)$_1$V$_3$-40]

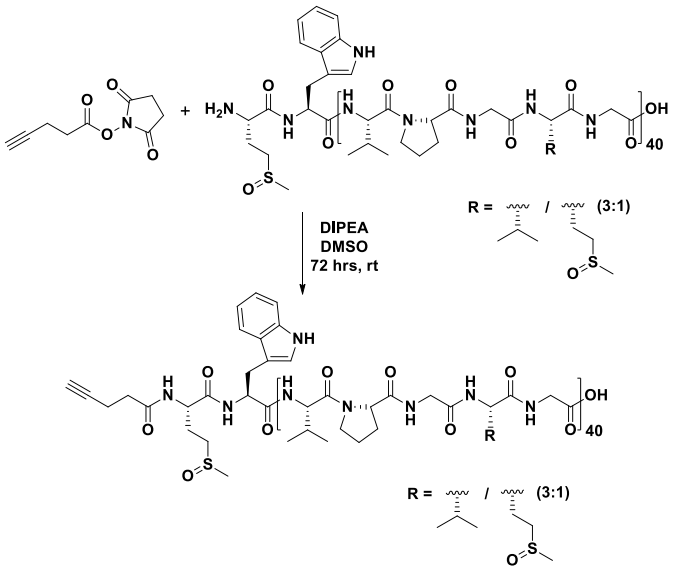

Scheme S2. Synthesis of *Alkyne*-ELP[M(*O*)$_1$V$_3$-*40*].

To a solution of ELP[M(*O*)$_1$V$_3$-*40*] (40 mg, 2.32 µmol) in anhydrous DMSO (2 mL) *N, N*-diisopropylethylamine (0.3 mg, 2.32 µmol) was added and followed by addition of 4-pentynoic acid succinimidyl ester (9 mg, 46.48 µmol). The reaction mixture was stirred for 72h under Ar at room temperature. Then the solution was diluted with 15 mL of water and dialyzed against ultrapure water in a dialysis bag (cut-off MWCO 3.5 kDa) for 72h by changing the water every 3h. The solution was lyophilized to yield *Alkyne*-ELP[M(*O*)$_1$V$_3$-*40*] (30 mg, 75%) as a white powder.

^{1}H NMR (400 MHz, D_2O, 25 °C): δ 4.29−4.23 (m, 80 H, αC*H* Val, Pro), 4.09−3.99 (d, 30 H, αC*H* VPGVG), 2.85−2.73 (m, 22 H, CH_2S Met), 2.38-2.29 (br m, γCH_2 Met, $CH_2CH_2C{\equiv}CH$), 2.56 (s, 33 H, SCH_3 Met), 0.82−0.75 (br m, 420 H, CH_3 Val).

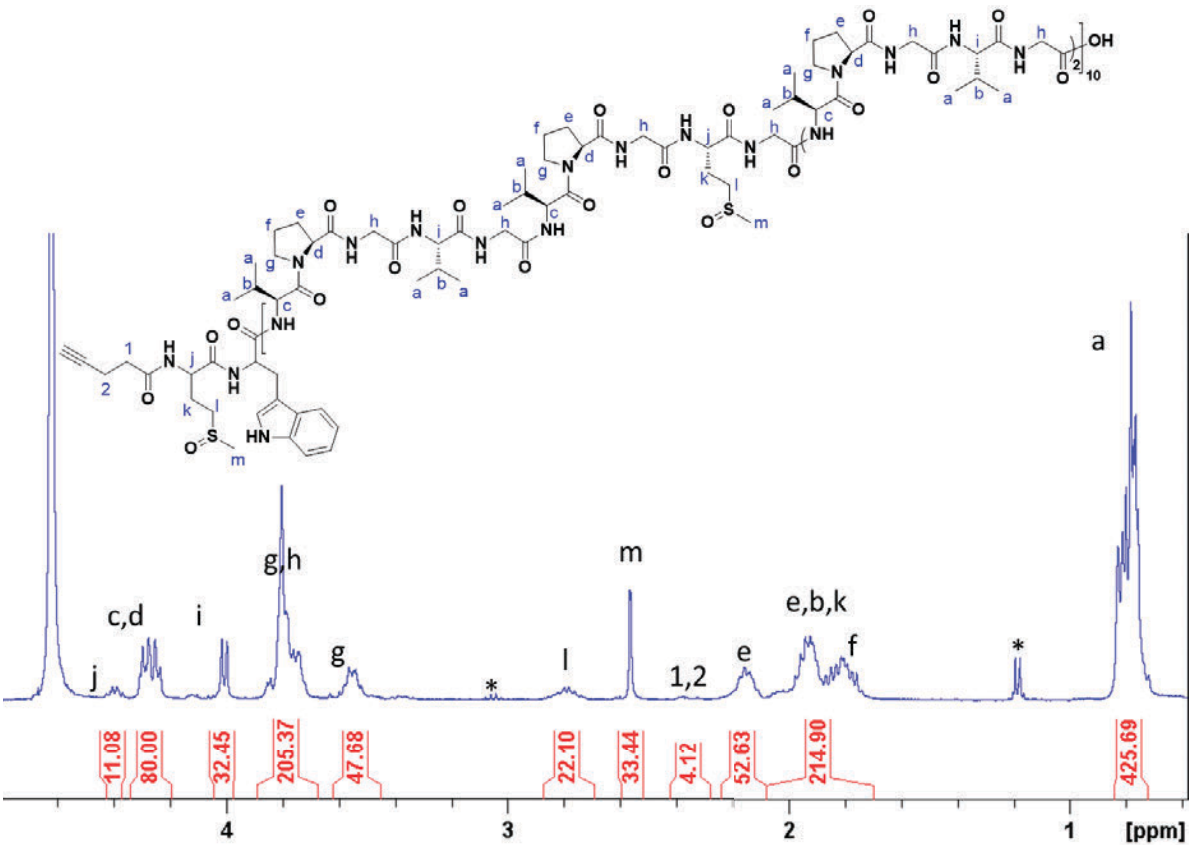

Figure S8. ^{1}H NMR spectrum of *Alkyne*-ELP[M(*O*)$_1$V$_3$-*40*] in D_2O at room temperature (*EtOH).

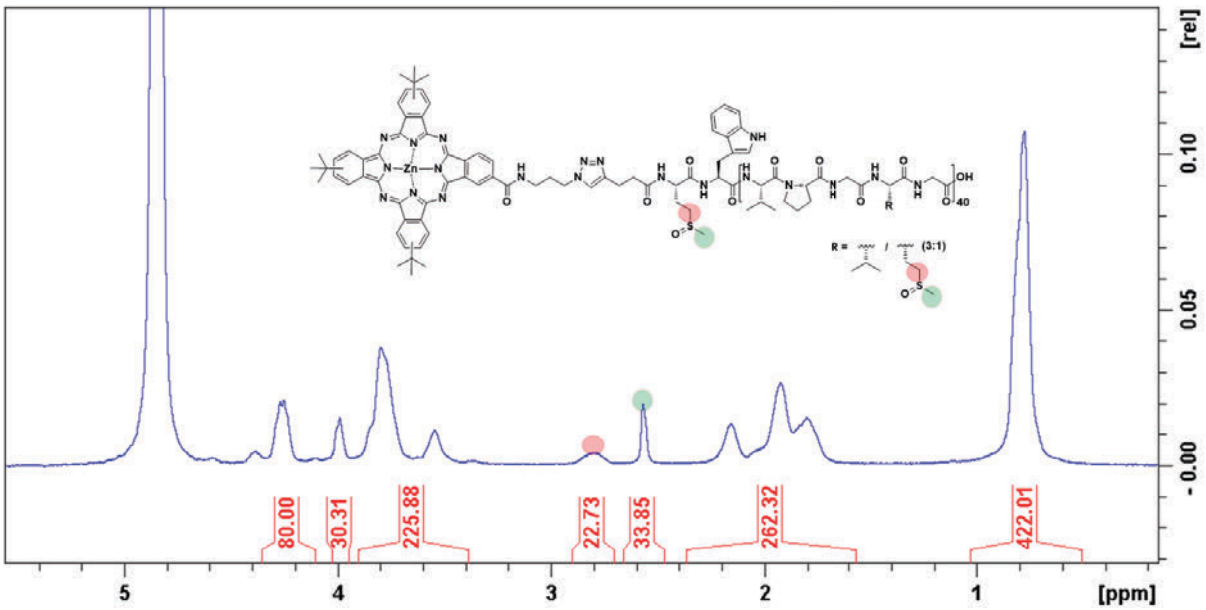

Figure S9. ^{1}H NMR spectrum of *TT1*-ELP[M(*O*)$_1$V$_3$-*40*] in D_2O at 5 °C.

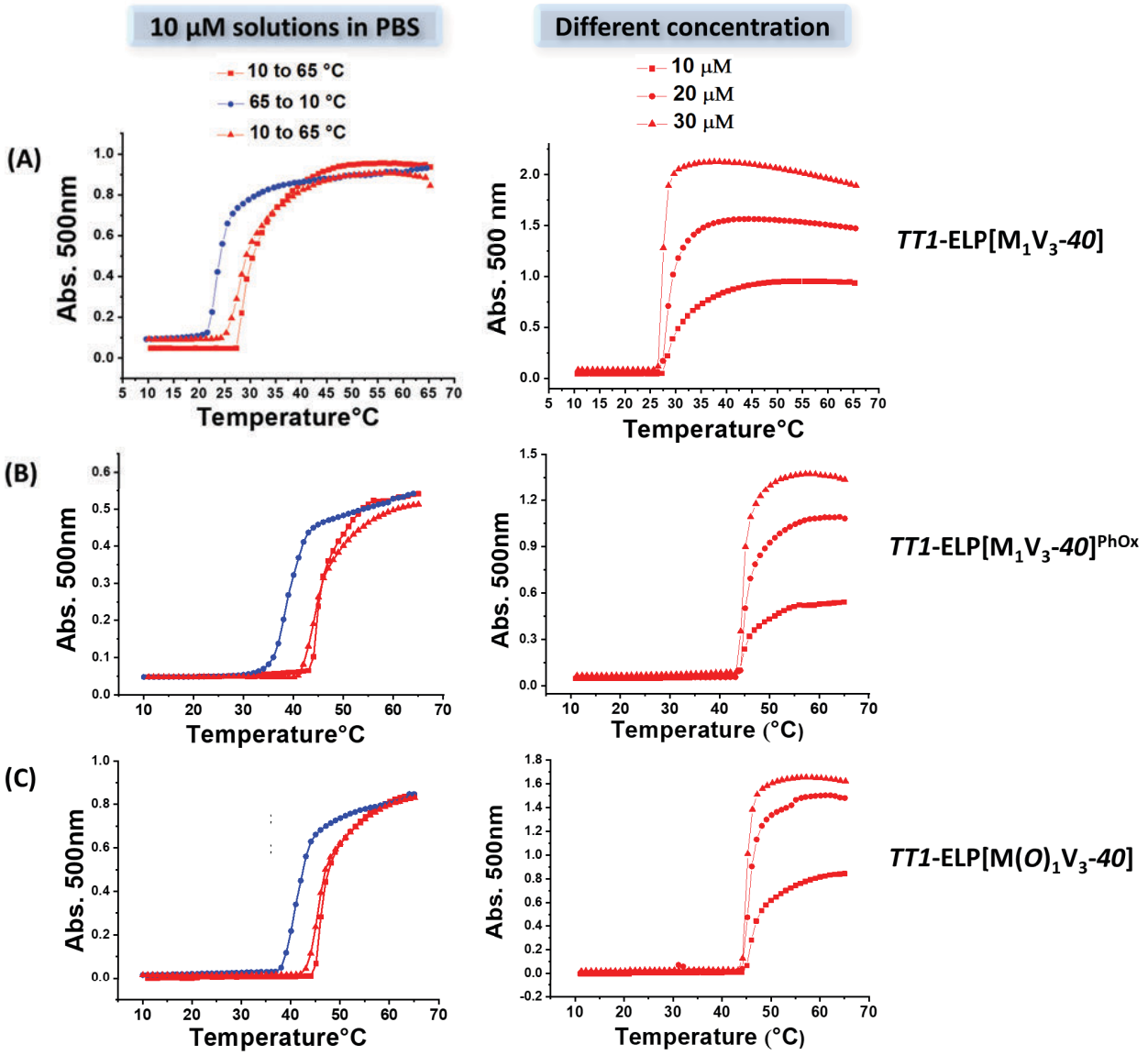

Figure S10. Absorbance (A.U.) at 500 nm of (A) *TT1*-ELP[M_1V_3-*40*], (B) *TT1*-ELP[M_1V_3-*40*] photooxidized, noted *TT1*-ELP[M_1V_3-*40*]^{PhOx}, and (C) *TT1*-ELP[M(*O*)$_1V_3$-*40*] solutions upon heating-cooling-heating (10-65 °C) cycles at 10 µM (left panels) and upon heating at 10 µM, 20 µM and 30 µM concentrations (right panels) in PBS as a function of temperature.

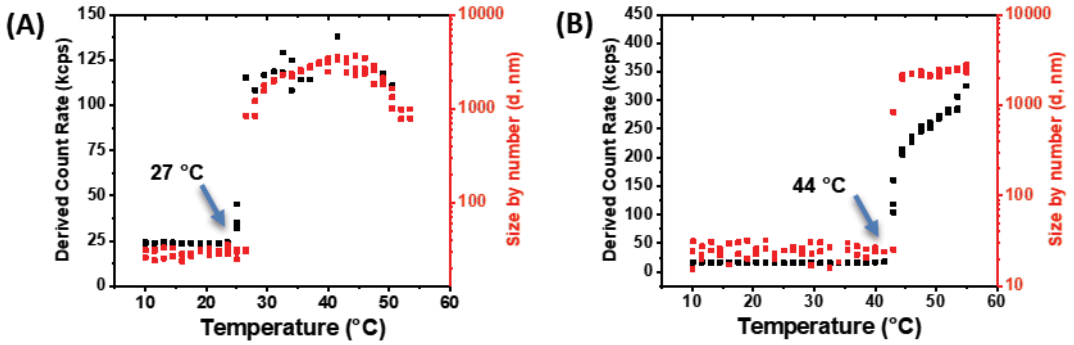

Figure S11. Temperature ramp results of (A) *TT1*-ELP[M_1V_3-*40*] and (B) *TT1*-ELP[$M(O)_1V_3$-*40*] solutions at 30 μM concentration in PBS buffer upon heating at a range of 10-55 °C (1.5 °C step, n=3) measured by DLS at 90° angle.

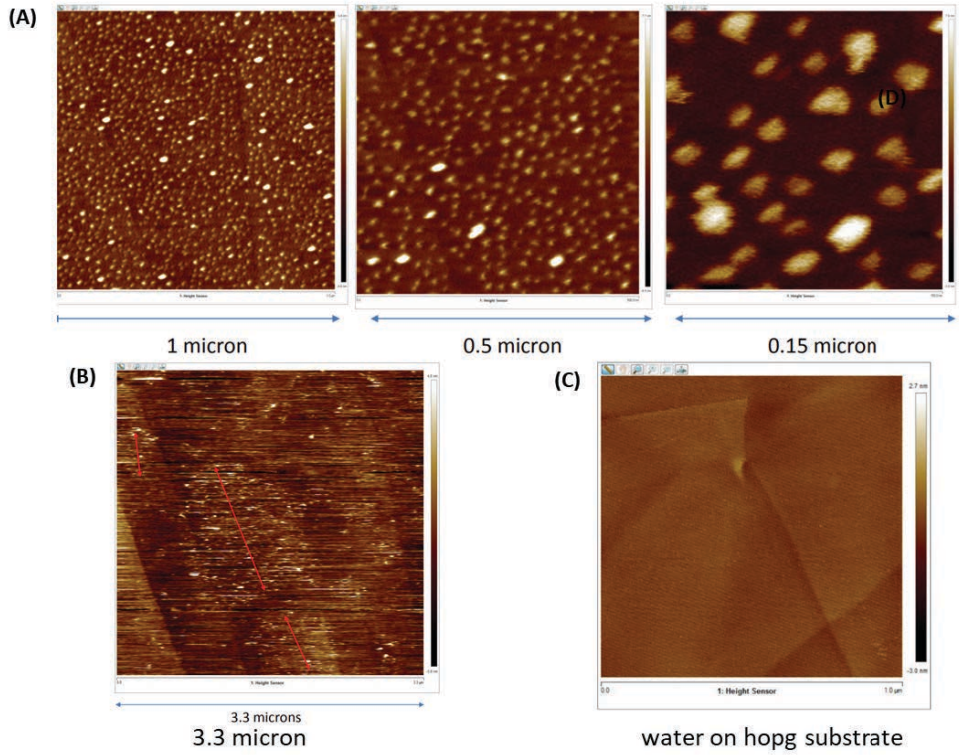

Figure S12. Temperature-Controlled High-Speed AFM (liquid) images of *TT1*-ELP[M_1V_3-*40*] on HOPG substrate (A) at 15 °C, (B) at 50 °C in PBS and (C) pure water on HOPG substrate.

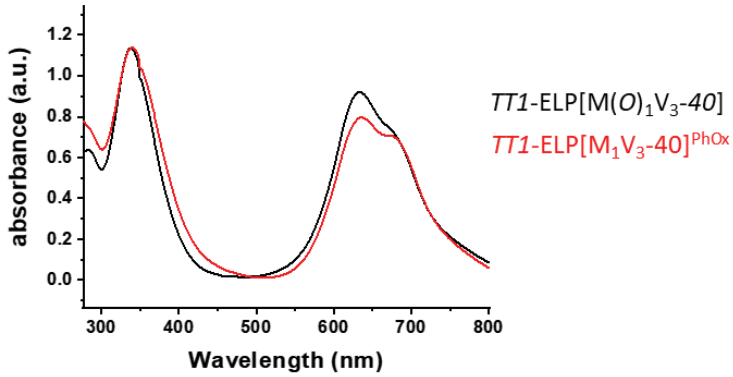

Figure S13. Overlapped absorption spectra of *TT1*-ELP[M(O)$_1$V$_3$-*40*] (black curve) and *TT1*-ELP[M$_1$V$_3$-*40*]^{PhOx} (red curve) in water.